



<https://theses.gla.ac.uk/>

Theses Digitisation:

<https://www.gla.ac.uk/myglasgow/research/enlighten/theses/digitisation/>

This is a digitised version of the original print thesis.

Copyright and moral rights for this work are retained by the author

A copy can be downloaded for personal non-commercial research or study, without prior permission or charge

This work cannot be reproduced or quoted extensively from without first obtaining permission in writing from the author

The content must not be changed in any way or sold commercially in any format or medium without the formal permission of the author

When referring to this work, full bibliographic details including the author, title, awarding institution and date of the thesis must be given

Enlighten: Theses

<https://theses.gla.ac.uk/>
research-enlighten@glasgow.ac.uk

**Calculation of potentials induced by stressors on
semiconducting heterostructures**

by

David Peticrew

**A Thesis submitted in partial fulfilment
of the requirements for the degree of**

MSc

University of Glasgow

September 1999

ProQuest Number: 10390881

All rights reserved

INFORMATION TO ALL USERS

The quality of this reproduction is dependent upon the quality of the copy submitted.

In the unlikely event that the author did not send a complete manuscript and there are missing pages, these will be noted. Also, if material had to be removed, a note will indicate the deletion.



ProQuest 10390881

Published by ProQuest LLC (2017). Copyright of the Dissertation is held by the Author.

All rights reserved.

This work is protected against unauthorized copying under Title 17, United States Code
Microform Edition © ProQuest LLC.

ProQuest LLC.
789 East Eisenhower Parkway
P.O. Box 1346
Ann Arbor, MI 48106 – 1346

Abstract

I have calculated the potential energy induced by stressors on the surface of a semiconducting heterostructure with $\bar{4}3m$ symmetry. The stressors may be single gates of arbitrary shape or one- and two-dimensional arrays of such gates, and I give results for an arbitrary surface. When the gates are metal, the strain arises from the differential thermal contraction of the gates and the substrate. Strain can also be induced by including a deliberately strained layer in the heterostructure and partly etching it away. The strain couples to the electrons by the deformation potential and the piezoelectric effect. The deformation potential does not depend on orientation but the piezoelectric effect usually dominates, and its angular dependence breaks the symmetry of the gate.

I provide direct results in real space for single stripe gates, which is useful because even fast Fourier transforms take time and computing power. I also provide results in Fourier space for arrays of stripe gates, single circular and square gates and two-dimensional arrays of such gates. I consider the (100), (110), (111) and (311) surfaces in detail. Of these, the (111) surface may prove to be attractive for experiments since the piezoelectric effect is both strong and approximately isotropic. Harnessing this potential has allowed a range of new experiments on lateral surface superlattices to be designed and carried out at Glasgow. These have utilised the piezoelectric effect to produce a potential that has half the period of the fabricated structure. The strong potential induced by the piezoelectric effect has also revealed new features in the transport through a superlattice. These calculations have also shown that the piezoelectric potential can no longer be ignored when designing or modelling structures built on piezoelectric semiconductors, which include GaAs and other III-V materials. I have shown that placing a gate on the surface will produce a potential of around 1 meV at a depth roughly equal to half the width of the gate, which will have a measurable effect on devices. I also show how the piezoelectric potential can be minimised or eliminated if possible.

List of Publications

"Theory of potential Modulation in lateral surface superlattices. III. Two-dimensional superlattices and arbitrary surfaces"

J. H. Davies, D. E. Petticrew, and A. R. Long, Phys. Rev. B **58**, 10789 (1998)

"Large periodic potential under lateral surface superlattices fabricated from heteroepitaxial stressor layers"

C. J. Emeleus, B. Milton, A. R. Long, J. H. Davies, D. E. Petticrew, and M. C. Holland, Appl. Phys. Lett. **73**, 1412 (1998)

"Piezoelectric potential under two-dimensional superlattices"

D. E. Petticrew, J. H. Davies, A. R. Long, I. A. Larkin, Physica B **249-251**, 900 (1998)

"Giant commensurability oscillations in a stressed surface superlattice"

C. J. Emeleus, B. Milton, A. R. Long, J. H. Davies, D. E. Petticrew, and M. C. Holland, Superlattices and Microstructures **25**, 29 (1999)

Acknowledgements

I would like to thank my supervisor John Davies for his help and persistence. I would like to thank Andrew Long, John Emeleus and Brian Milton for discussions about ongoing experiments.

This work was supported by EPSRC.

Table of Contents

1	Introduction	1
1.1	Potentials from a surface structure	1
1.2	Heterostructures	2
1.3	Experimental systems	3
1.4	Weiss oscillations	4
1.5	Effect on FETs	7
1.6	Synopsis	8
2	Physical Model	10
2.1	Physical system	10
2.2	Elastic model	12
2.3	Piezoelectric effect	14
2.4	Electrical model	16
2.5	Deformation potential	17
3	Single Stripe Gate	19
3.1	Strain field	19
3.2	Deformation potential	22
3.3	Piezoelectric potential on [100]	23
3.4	Piezoelectric potential on different surfaces	26
3.5	Results	28
3.6	Conclusions	32
4	One-dimensional Lateral Surface Superlattices	34
4.1	Extension to Lateral Surface Superlattices	34
4.2	Comparison with experiments	35
4.3	Conclusions	39
5	Island Gates	40
5.1	Elastic model	40
5.2	Deformation potential	44
5.3	Piezoelectric potential	45
5.4	Piezoelectric potential in real space	46
5.5	Piezoelectric potential in Fourier space	49
5.6	Piezoelectric potential on an arbitrary surface	50

Table of Figures

Figure 1 A general surface structure on the surface of a semiconductor	1
Figure 2 Self-consistent solution of the conduction band $E_c(z)$ through modulation-doped layers with no gate bias $v_G = 0.2$ V and $n_{2D} = 3 \times 10^{15}$ m ⁻² electrons in the 2DEG.....	3
Figure 3 A 1D LSSL and a 2D LSSL. The gates are grey, the semiconductor is red and the 2DEG is blue.	4
Figure 4 Experimental result for magnetoresistance as a function of magnetic field B . The commensurability oscillations occur for $B < 0.5$ T, and show a strong second harmonic content. This is confirmed by the power spectral density (PSD inset) obtained from a Fourier transform of the magnetoresistance considered as a function of $1/B$. The peaks at low frequency arise from commensurability oscillations, showing a strong fundamental and second harmonic but a little third harmonic; the peak at 7-8 T is from the Shubnikov-de Haas effect. A positive magnetoresistance peak at 0.1 T can also be seen.....	6
Figure 5 Possible trajectories for an electron moving in a magnetic field and a sinusoidal potential. The horizontal lines are equipotentials at $y/2b$, where b is the period of the potential, blue is a negative potential and red is positive. On resonance, the guiding-centre drift is maximal; off rsonance, the drift is negligible.....	5
Figure 6 The layers for the stressor	10
Figure 7 Self-consistent solution of the conduction band $E_c(z)$ through modulation-doped layers with no gate bias $v_G = 0$ V. Both the 2DEG and the parasitic layer of electrons around the donors can be seen clearly.....	11
Figure 8 Axes used.....	12
Figure 9 Screened piezoelectric potential energy in 2DEG's, at a depth of 50 nm with no parasitic layer, under stripe gates of width 100 nm on various surfaces. Curves are offset for clarity with the corresponding zero's shown as dashed lines. The deformation potential energy is also shown for comparison.....	30
Figure 10 Approximations to the screened piezoelectric potential energy in a 2DEG, at a depth of 50 nm with no parasitic layer, under a stripe gate of width 100 nm. Curves are offset for clarity with the corresponding zero's shown as dashed. The	

d/dz approximation is shown along with the exact Thomas Fermi screening and a further approximation where the exponential term is neglected in Thomas Fermi screening.....31

Figure 11 A section of a one-dimensional LSSL, made by etching InGaAs layers.

Purple - GaAs, Red - AlGaAs, Yellow - Delta doped AlGaAs, Blue - InGaAs...34

Figure 12 Magnetoresistance of four Hall bars with stressed superlattices of different orientations. Curves are offset for clarity as follows: $[01\bar{1}] +50 \Omega$; $[010] +100 \Omega$; and $[011] +150 \Omega$. The temperature was 5.1 K to suppress Shubniko-de Haas oscillations. The strong dependence on orientation is a signature of the piezoelectric effect. The magnetoresistance of an unstressed $[01\bar{1}]$ control sample is shown by the dashed blue line and depends only weakly on orientation.38

Figure 13 A general surface structure of the surface of a semiconductor.....40

Figure 14 Some of the forces for the elastic model of gate.41

Figure 15 Piezoelectric charge density in a plane 50 nm below a (100) surface due to point forces at the origin, aligned along the $[010]$ crystal axis, the $[011]$ direction, the $[001]$ crystal axis and the $[0\bar{1}1]$ direction. Each plot shows an area of $(200 \text{ nm})^2$. Blue is negative charge density, which leads to a positive potential energy and red is positive charge density.47

Figure 16 Screened piezoelectric potential energy in a 2DEG situated 50 nm below circular gates of diameter 100 nm (black outline) on different surfaces. The scale goes from -1.5 meV (blue) through 0 meV (white) to $+1.5 \text{ meV}$ (red).....54

Figure 17 Screened piezoelectric potential energy in 2DEG's of different depths under a circular gate of diameter 100 nm on a (100) surface (thick lines). The radius is along $[010]$, where the piezoelectric effect reaches its maximum. Curves are offset for clarity as shown by horizontal lines. The effect of additional screening by a parasitic layer of electrons around the donors, 25 nm deep, is shown for the 50-nm depth (broken thick orange line). The screened deformation potential energy (thin purple line) has circular symmetry, and the corresponding bare energy (thin dotted cyan line) is proportional to the dilation; both are for a depth of 50 nm with no parasitic layer.55

Figure 18 A section of a two-dimensional LSSL, with circular gates, made by etching InGaAs layers. Purple - GaAs, Red - AlGaAs, Yellow - Delta doped AlGaAs, Blue - InGaAs.....58

Figure 19 A section of a two-dimensional LSSL, in chessboard layout i.e. square gates touching at the corners, made by etching InGaAs layers. Purple - GaAs, Red - AlGaAs, Yellow - Delta doped AlGaAs, Blue - InGaAs. 60

Figure 20 Screened piezoelectric potential in a 2DEG of depth 50 nm below arrays of gates on a (100) surface. They are aligned to the crystal axes in (a) and (b) and to the cleavage planes in (c) and (d). The gates (black outline) have width or diameter of 100 nm in a square array of period 200 nm. The scale goes from -1 meV (blue) through 0 meV (white) to +1 meV (red). 62

Figure 21 Screened piezoelectric potential in a 2DEG of depth 50 nm below array of gates on a (100) surface. The gates (black outline) have a width of 100 nm in a square chess board array of period 200 nm and the scale goes from -1 meV (blue) through 0 meV (white) to +1 meV (red). 63

1 Introduction

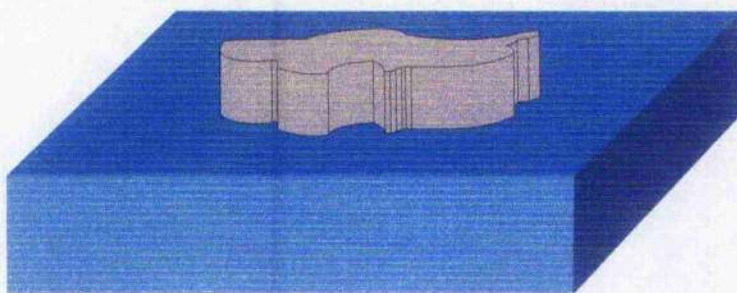


Figure 1 A general surface structure on the surface of a semiconductor

1.1 Potentials from a surface structure

While semiconductors are important in modern electronics, a lump of homogeneous semiconductor has limited uses. Often the semiconductor is patterned by structures on the surface. These structures are then used to produce potentials in the semiconductor, which can either confine or guide electrons or holes. This potential can arise from various sources. One source that has previously received little attention is strain. However, recent experiments and calculations have shown the importance of strain when characterising or designing devices, particularly in III-V compounds where the piezoelectric effect produces large potentials¹⁻⁷.

The strain can arise from several sources. If the surface structure is another semiconductor then strain can arise from a mismatch in the lattice constants of the two semiconductors. When the surface structure is a metal gate, then strain can arise if the sample is cooled and the metal contracts at a different rate to the semiconductor^{2,3}. This strain leads to a potential in the semiconductor through two effects, either directly shifting the energy of the bands that the holes and electrons exist in resulting in the deformation potential³ or by causing a polarisation of the semiconductor atoms resulting in a piezoelectric potential⁸. I have investigated the potentials arising from strain, due to surface gates of various geometries including stripe, square, and circular gates, both in isolation and in arrays^{10,11}.

The potentials arising from the strain, however, depend not only on the nature and shape of the surface structures but also on the underlying semiconductor. While I calculate the strains and potentials arising when the semiconductor considered is just a

homogeneous block, I am mainly interested in the effect on a two-dimensional electron gas in a heterostructure. Thus, the main results of each section are the potential energy arising in such a system. I will also show how these results can be used to design systems to either eliminate these potentials or minimise them. In addition, I will also show how to engineer systems to take advantage of these potentials by maximising their effect or eliminating certain harmonics from them.

1.2 Heterostructures

A heterostructure is any semiconductor composed of more than one material. Different semiconductors have different band energies and different lattice constants, it is therefore possible to design and build heterostructures to control the motion of the electrons and holes in the semiconductor. This is called band engineering¹².

If the layers in a heterostructure are grown so that there is one potential well in the conduction band below the Fermi energy, the maximum energy allowed for an electron in the system, then all the electrons will be trapped in this well. If the temperature is lowered sufficiently and the density of states is sufficiently low, then all the electrons will lie in one quantum mechanical state perpendicular to the surface of the semiconductor, although they remain free in a plane parallel to the surface of the semiconductor. Such a system is called a two-dimensional electron gas (2DEG), a typical example of which can be seen in Figure 2^{12,13}. A 2DEG has several advantages over a general n-type semiconductor; the mobility is much higher, the mean free path is longer, typically around 20 μm and the electron density is much higher. The 2DEG's considered here are made from GaAs/AlGaAs heterostructures because they offer a larger mobility than their Si counterparts¹⁴.

Another feature that can be used when constructing these devices is δ -doping¹⁴. This is when instead of having a doped slab of semiconductor grown in the heterostructure, a doped layer is grown. In this way, all the donors are confined to a plane. This allows the 2DEG to be grown shallower so that a potential applied at the surface is attenuated less when it reaches the 2DEG than for the equivalent slab doped heterostructure. If the density of donors is too high then the energy can dip below the Fermi energy and give rise to a parasitic layer of electrons in the donor layer¹⁵, as shown in Figure 7. This effect has important consequences for the potential energy in the 2DEG, since it

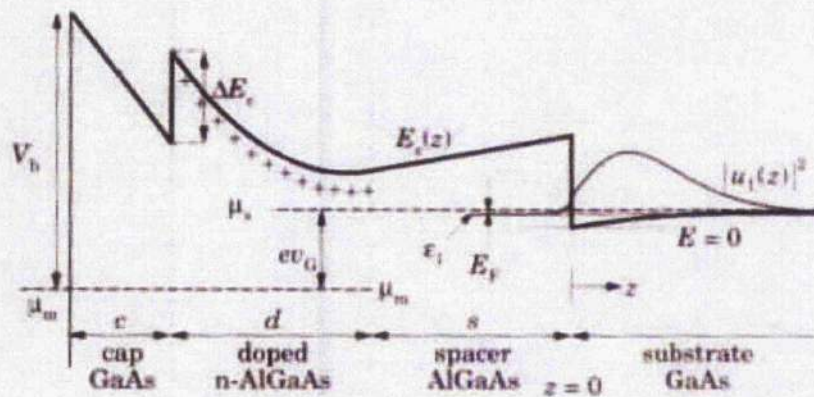


Figure 2 Self-consistent solution of the conduction band $E_c(z)$ through modulation-doped layers with no gate bias $v_G = 0.2 \text{ V}$ and $n_{2D} = 3 \times 10^{15} \text{ m}^{-2}$ electrons in the 2DEG. The 2DEG is shown as $|u_1(z)|^2$.

[Modelling program courtesy of Prof. G. L. Snider, University of Notre Dame.]

Figure 9.1 from Davies¹²

increases the screening and can act as an equipotential plane between the 2DEG and the surface. However, these electrons are not totally free to move and remain bound to the donors. It is however, a reasonable approximation to treat some of the electrons as free when calculating the screening, this will be dealt with in §2.4.

1.3 Experimental systems

The primary experimental system for which these potentials have been devised is the lateral surface superlattice (LSSL). This is an array of gates on top of a heterostructure with a 2DEG. A one-dimensional LSSL is an array of stripe gates and a two-dimensional LSSL is an array of either circular or square gates, as shown in Figure 3. These devices were originally fabricated to look for quantum mechanical effects such as Bloch oscillations, where the electrons oscillate instead of continually increasing their kinetic energy as they would in a classical system, and the Hofstadter butterfly, a remarkable self similar pattern produced by the splitting of the Landau levels by a two-dimensional periodic potential and a magnetic field¹⁶. However, the periods of potential that can be currently fabricated are too large to observe any of these effects, instead semi-classical effects were observed. Two of these effects have been

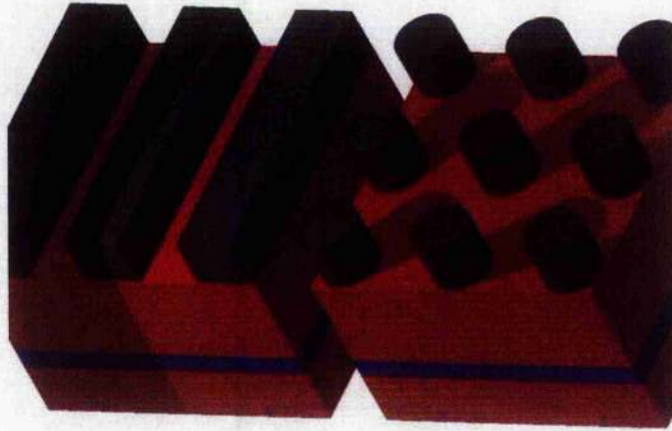


Figure 3 A 1D LSSL and a 2D LSSL. The gates are grey, the semiconductor is red and the 2DEG is blue.

explained for a one-dimensional LSSL, Weiss oscillations¹⁷⁻²¹, for $B < 0.5$ T and a positive magnetoresistance (PMR) peak at $B \approx 0.1$ T^{23,24}. Both of these effects can be used to measure the potential in the 2DEG, while the Weiss oscillations can be used to measure the harmonic content of the potential².

1.4 Weiss oscillations

When the electrons in a 2DEG are subjected to a perpendicular magnetic field then they move in circles called cyclotron orbits, the radius of which is given by $R_c = mv_F / eB$, where v_F is the Fermi energy, e is the electronic charge and m is the effective mass of the electrons in the substrate. If in addition to the perpendicular magnetic field the electrons are subjected to a periodic electric field from a 1D LSSL, then the interplay between the cyclotron orbit and periodicity of the potential produces some commensurability effects [Figure 5]. One such effect is commensurability oscillations in the magnetoresistance of the 2DEG¹⁷, first discovered by Weiss, von Klitzing, Ploog and Weimann¹⁷. At low magnetic fields (< 0.5 T at 4.5K) there are oscillations in the magnetoresistance which are periodic in $1/B$. These oscillations were explained semi-classically by Beenakker²².

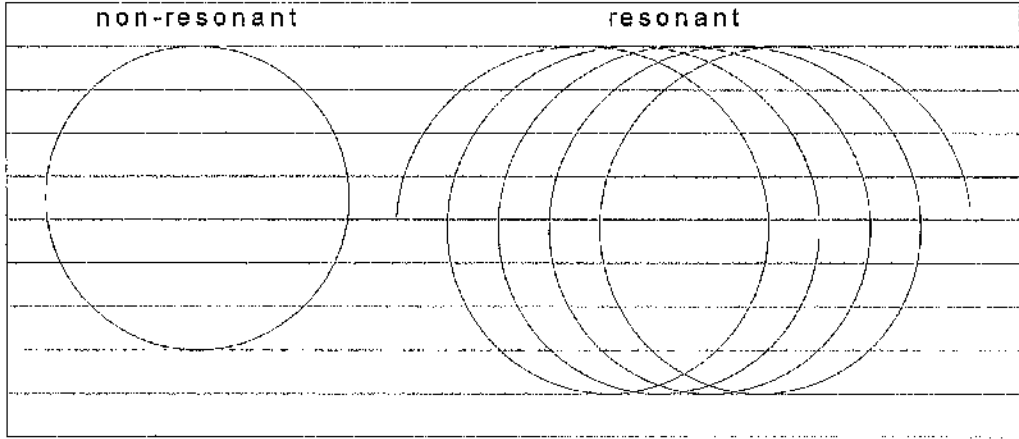


Figure 4 Possible trajectories for an electron moving in a magnetic field and a sinusoidal potential. The horizontal lines are equipotentials at $y/2b$, where b is the period of the potential, blue is a negative potential and red is positive. On resonance, the guiding-centre drift is maximal; off resonance, the drift is negligible.

If the potential is small, then the motion of the electrons can be considered a perturbation of the cyclotron orbits produced by a magnetic field alone. This is done by considering the motion of the centre of the cyclotron orbit or guiding centre. When the effect of the periodic potential is averaged over the path of the electron (the cyclotron orbit), it is found that for most of the orbit there is no net effect, since the electron passes over a full period and the forces cancel. This however does not hold at the edges of the orbit when the electron does not cross a full period. Therefore, when the signs of the potential for the extremities of the cyclotron orbit are the same the drift velocity is enhanced and when the signs are opposite the drift velocity is diminished to zero and the electrons just orbit as in the absence of a potential [see Figure 4]. On solving the semi-classical Boltzmann equation, Beenakker was able to find this approximate expression for the oscillations in the magnetoresistance.

$$\frac{\rho_{xx}}{\rho_0} = 1 + 2V^2 \frac{l^2}{bR_c} \cos^2(2\pi R_c/b - \pi/4), \quad (1.1)$$

where ρ_{xx} is the resistance measured by the current in the x direction of a hall bar when a voltage is applied in the x direction and ρ_0 is the resistance of the sample at zero magnetic field, V is the magnitude of the potential in the 2DEG, E_F is the Fermi energy, b is the period of the potential and l is the mean free path.

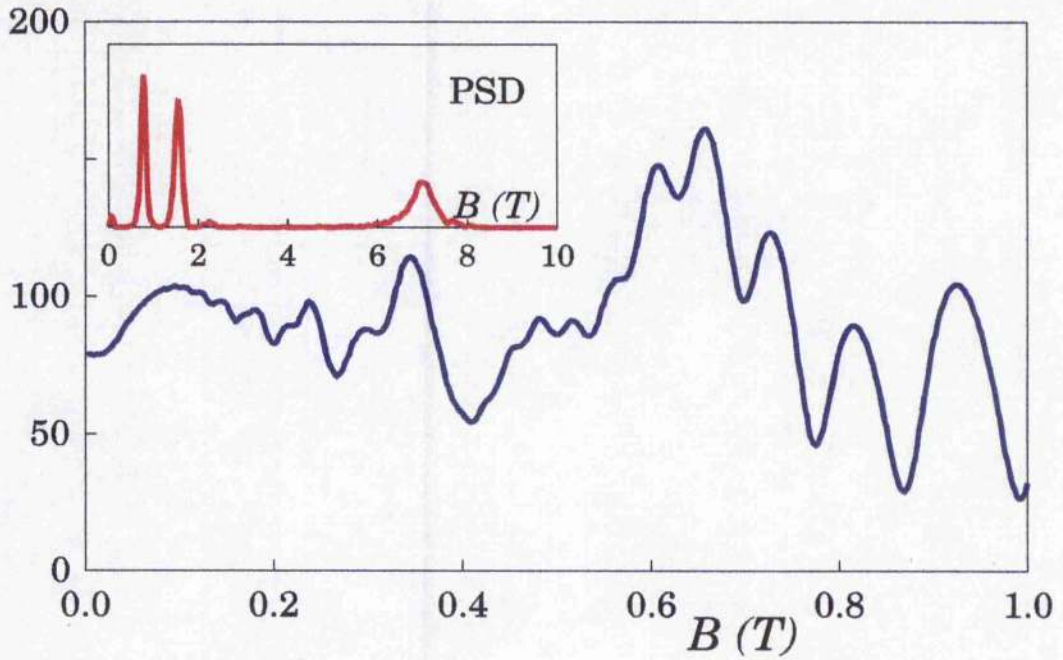


Figure 5 Experimental result for magnetoresistance as a function of magnetic field B . The commensurability oscillations occur for $B < 0.5$ T, and show a strong second harmonic content. This is confirmed by the power spectral density (PSD inset) obtained from a Fourier transform of the magnetoresistance considered as a function of $1/B$. The peaks at low frequency arise from commensurability oscillations, showing a strong fundamental and second harmonic but little third harmonic; the peak at 7-8 T is from the Shubnikov-de Haas effect. A positive magnetoresistance peak at 0.1 T can also be seen.

[Figure from Davies and Larkin³]

This result was later generalised by Gerhardt to include higher harmonics²⁵.

$$\frac{\rho_{xx}}{\rho_0} = \sum_{n=1}^{\infty} \left(\frac{V_n}{E_F} \right)^2 \frac{nl^2}{aR_c} \cos^2 \left(\frac{2\pi nR_c}{a} - \frac{\pi}{4} \right), \quad (1.2)$$

where V_n is the magnitude of the n th harmonic of the potential in the 2DEG. This result can be used to determine the square of the Fourier components of a periodic potential by analysing the magnetoresistance. Unfortunately, this does not give the sign of the Fourier components.

However, there are some problems with this theory. While it correctly identifies the position of the peaks, it gets most of the amplitudes wrong. This is thought to arise due to only considering isotropic scattering. This has been considered by Mirlin and Wolfe²⁶ semiclassically, and by others quantum mechanically^{27,28}, however the results they give are not as amenable to a straightforward interpretation of the data as Beenakker's result. Several authors have also looked at this issue numerically²⁹.

Gerhardt has attempted to extend the results for a one-dimensional LSSL to a two-dimensional LSSL^{25,30}. He proposes that the addition of a second perpendicular periodic potential has no effect on the magnetoresistance measured perpendicular to the original periodic potential. It only introduces additional commensurability oscillations when the magnetoresistance is measured perpendicular to the new periodic potential. However, recent experimental and theoretical work has cast doubt on this³¹. Although there has been an attempt to look at the two-dimensional case quantum mechanically³² it is still not yet understood and needs to be investigated further. It is hoped that the calculation of the two-dimensional potentials will facilitate this investigation.

1.5 Effect on FETs

These potentials also have applications in some devices. While this work demonstrates that strain should be considered in all surface structures, it is particularly applicable to surface structures in GaAs/AlGaAs where the piezoelectric coupling of the strain to the electrons induces a strong potential. However, the devices to which my work are most easily applicable are FETs particularly MODFETs. Since a MODFET is effectively just a gate with a 2DEG beneath it, the results for single stripe gates are directly applicable.

Although some results exist for arrays of gates on (100) these require a lot of Fourier components to be included for an accurate calculation when reduced to a single gate. It is desirable to have a simple expression in real space for potentials produced by a single gate.

Strain potentials give rise to a number of observable effects in FETs, the most prominent of which is a shift in the threshold voltage³³. This arises straightforwardly as potentials arising from the strain in the gates shift the energies of the electrons in the 2DEG, sometimes by as much as a few meV, thus requiring a different voltage to remove the electrons from the channel³³. Sometimes it is desirable to minimise these strain effects while at other times it could be useful to harness the built in potential generated. It is therefore a goal to find the conditions under which this can be achieved.

The first work in this area was carried out by Asbeck et. al.³³. They recognised the dominance of the piezoelectric effect in the shift of the threshold voltage of FETs. They were able to calculate the charge density produced by a gate aligned to the cleavage planes on a (100) surface. They also deduced from this the change in the threshold voltage of a FET, however they gave no expression for either the potential produced by this system or the effect on a 2DEG. I will therefore calculate the potentials arising from single gates as well as arrays of gates.

1.6 Synopsis

In chapter 2 I consider the physical model and establish the elastic and electrostatic models, the approximations and the assumptions I will use.

Then in chapter 3 I calculate the strain fields produced by a single stripe gate. For one-dimensional stripe gates, this is done by considering a two-dimensional elastic potential. I can then calculate the charge density produced via the piezoelectric tensor. This must be rotated to the correct orientation first. This rotation of the piezoelectric tensor is responsible for the angular dependence of the resulting charge densities and potentials. Once I have the charge densities for the stripe gates, I then calculate the potential using Poisson's equation. I then screen it using an approximation to Thomas Fermi screening to allow for the presence of the 2DEG and any nearby equipotential planes. I thus calculate an expression for the screened potential in a 2DEG in real space.

In chapter 4 I calculate the potential arising from an array of gates, or lateral surface superlattice by Fourier transforming the potential and then limiting the Fourier wave vector to certain values.

In chapter 5 I consider the potential produced by island gates. The situation becomes more complex and a three-dimensional elastic potential is required. Therefore, I have abandoned the approach of chapter 3 for the two-dimensional case and used the superimposition of the results for point forces, instead. The foundation of this work is the displacement from a point force, which was solved by Cerruti. This is then used to calculate the strain. The piezoelectric tensor is then used in like manner to the stripe gate to calculate the charge density. It is hard to proceed from here in real space, so the quantities are Fourier transformed. The potential can then be calculated and screened giving the potential in the 2DEG. I also introduce the idea of a pseudopotential derived from the displacement, which simplifies multiple calculations on different surfaces.

I then extend these results in chapter 6 to consider the case of two-dimensional LSSLs by limiting the Fourier wave vectors of the potentials to certain values.

Then in chapter 7 I present my conclusions and some of the experimental applications of my work and some suggestions for future work.

2 Physical Model

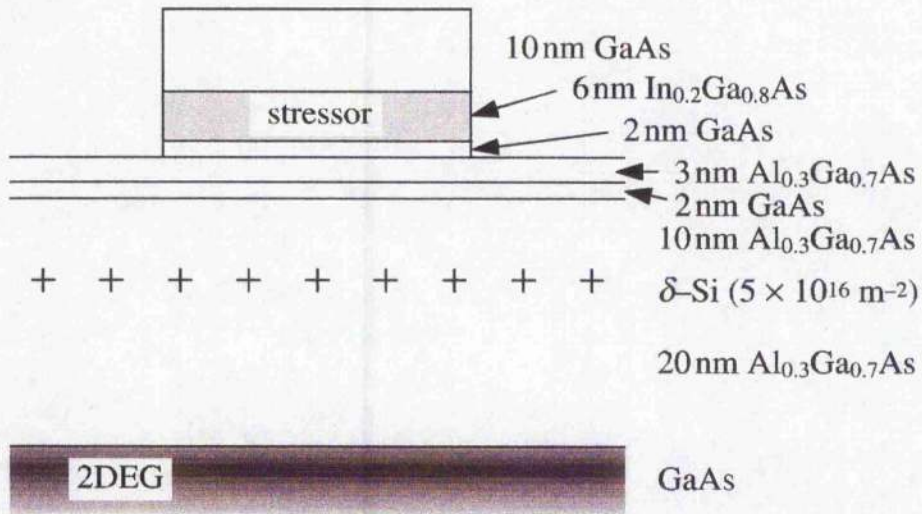


Figure 6 The layers for the stressor

2.1 Physical system

A heterostructure is grown on top of a GaAs substrate as shown in Figure 6. This modifies the conduction band of the semiconductor to trap electrons in one plane at the junction of the heterostructure and the substrate, as can be seen from Figure 7. This plane of electrons is called a 2-dimensional electron gas or 2DEG. While the confinement to one plane is simplistic, and in reality the electrons are in a quantum mechanical state spread over a depth of around 7 nm, the plane approximation is a good one and used here¹². The depth used for the 2DEG is taken as an average value.

On top of this heterostructure, another structure is placed on the surface. This can either be a metal gate or a stressor layer as shown in Figure 6, which can be etched to produce stripes and other patterns. These structures are referred to as gates for simplicity throughout the rest of this document, although the stressor layers are strictly not gates. Their elastic behaviour differs only in the sign and magnitude of the effect and will be treated with the same methods⁴.

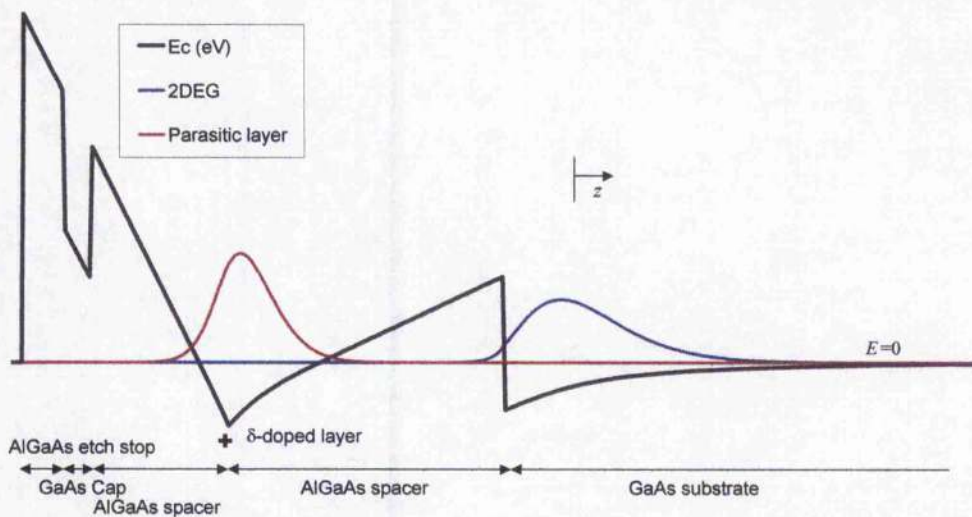


Figure 7 Self-consistent solution of the conduction band $E_c(z)$ through modulation-doped layers with no gate bias $v_G = 0$ V. Both the 2DEG and the parasitic layer of electrons around the donors can be seen clearly.

[Modelling program courtesy of Prof. G. L. Snider, University of Notre Dame.]

The choice of axes is awkward, because it is most convenient for the calculation to have z pointing into the substrate, whereas the conventional specification of a surface is by the outward normal. The outward normal is used to avoid confusion over the orientation, as shown in Figure 8. Equations will be written with $|z|$ to avoid misleading signs. The exposed surface of the semiconductor defines the plane $z = 0$

Table 1 Notation for orientation of crystal axes

Outward normal to the surface	Principal direction in plane of surface ($\theta = 0$)	Third axis ($\theta = 90^\circ$)
z	x	y
[100]	[010]	[001]
[110]	[001]	[1 $\bar{1}$ 0]
[111]	[01 $\bar{1}$]	[$\bar{2}$ 11]
[311]	[01 $\bar{1}$]	[$\bar{2}$ 33]

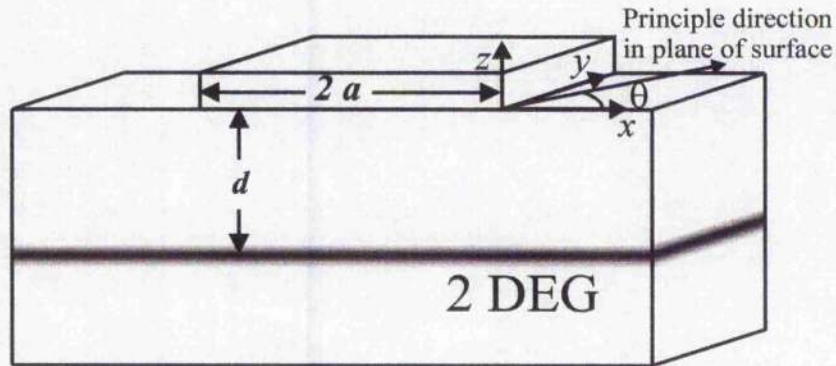


Figure 8 Axes used.

and x is chosen as the principle direction in this surface. Table 1 gives the notation for the surfaces that are considered.

The figures included are for a 2DEG of depth $d = 50$ nm in layers that are δ doped with a plane of donors at depth $c = 25$ nm. Results will be presented for circular and square gates with a diameter or width of $2a = 100$ nm, either isolated or in square arrays of period $b = 200$ nm. Finally, the one-dimensional superlattices have equal gates and gaps of 100 nm, giving a period of 200 nm.

2.2 Elastic model

In a metal gate, the stress arises from the thermal contraction that occurs when the semiconductor and the gate are cooled down to the measurement temperature e.g. 4.2K. However, the coefficients of the thermal expansion are different for the metal and the semiconductor. This differential thermal contraction strains the gate and the semi-conductor below it³.

The semiconductor is assumed to be a semi-infinite solid. It is also assumed to be homogenous and thus the elastic properties are assumed to be the same throughout, although in reality they differ in the different layers of the heterostructure. This is a reasonable approximation for AlGaAs and GaAs and it is hard to relax this approximation in analytical work. Similarly, the semiconductor is also assumed to be isotropic for elastic purposes. This is definitely not a good approximation for a semi-

conductor with $\bar{4}3m$ symmetry, like GaAs and AlGaAs. Again however, it is difficult to do better analytically.

I consider two models for the distribution of stress in the gate, both given by Larkin et. al.⁸ but modified for single gates rather than superlattices, the elastic and the rigid gate models. Both these models assume that the gate is thin enough so that it exerts no normal forces on the surface of the semiconductor.

1. The elastic gate is the limit of a thin gate, such that the lattice constant parallel to the surface in the gate is forced to match that of the underlying substrate. Thus the gate is in constant stress, and only exerts a force along the edges of the gate. This model is applicable when the thickness of the gate is very small compared to the width of the gate.
2. The rigid gate is the limit of a thick gate, such that the lattice constant in the substrate, directly beneath the gate, is forced to match that of the gate. Thus, on the surface of the substrate σ_{xx} is constant underneath the gate. This is applicable to a gate where the thickness of the gate is much larger than the width of the gate.

The force distribution for these models is obviously unrealistic and should be spread over the width of the gate⁹. However this is hard to model accurately⁸ especially for a two-dimensional gate. The rigid gate is the better model for the experimental system under consideration. However it is mathematically more complex than the elastic gate⁸. While either gate can be treated with the Airy stress functions used in Chapters 3-4, the more complicated island gates of Chapters 5-6 use the elastic gate model and so this model is used for most calculations for comparison purposes. The effect of the different models is only on the harmonic content of the potentials and does not effect the symmetry of the potentials.

The differential thermal contraction of a Ti gate on a GaAs substrate strains the gate by about +0.001, which generates a stress $\sigma_g = \epsilon_g E / (1 - \nu^2) \approx 0.15 \text{ GPa}$, where ν is Poisson's ratio and E is Young's modulus³⁴. These gates have a typical thickness $h = 30 \text{ nm}$, and the force per unit length at the edge of the gate is the product of these, $\bar{F} = -h\sigma_g \approx -5 \text{ Nm}^{-1}$; the sign shows that this is directed toward the centre of the

gate³. In a stressor layer, the stress is caused by a lattice mismatch between the stressor (InGaAs in Glasgow experiments) and the AlGaAs/GaAs, and gives rise to a strain of around -0.002 for a 20% InGaAs channel of width 6nm. These gates have a typical thickness of $h = 18 \text{ nm}$ ⁴.

The strain is defined to be

$$\varepsilon_{ij} = \frac{1}{2} \left(\frac{\partial u_i}{\partial R_j} + \frac{\partial u_j}{\partial R_i} \right) \quad (2.1)$$

where u_i is the displacement⁵.

The standard stress/strain equations for an isotropic medium, which are used throughout, are

$$\begin{aligned} E\varepsilon_{xx} &= \sigma_{xx} - \nu(\sigma_{yy} + \sigma_{zz}) \\ E\varepsilon_{yy} &= \sigma_{yy} - \nu(\sigma_{zz} + \sigma_{xx}) \\ E\varepsilon_{zz} &= \sigma_{zz} - \nu(\sigma_{xx} + \sigma_{yy}). \end{aligned} \quad (2.2)$$

Due to the homogeneous approximation ν and E are assumed constant throughout the heterostructure. Poisson's ratio is given by $\nu = 0.31$ ¹. This value of ν is appropriate for tensile stress along the principal axes. I use a value of $E = 90 \text{ GPa}$ for Young's modulus¹.

2.3 Piezoelectric effect

If semiconductors with $\bar{4}3m$ symmetry, including AlGaAs/GaAs, are strained, this produces a polarisation as the electrons and nuclei are separated. This polarisation is given by

$$P_i = d_{ijk} \sigma_{jk}, \quad (2.3)$$

where d_{ijk} is defined by this expression to be the piezoelectric tensor. There is also an alternative definition for an alternative piezoelectric tensor e_{ijk} , which relates the polarisation to the strain by

$$P_i = e_{ijk} \varepsilon_{jk}. \quad (2.4)$$

The piezoelectric tensors are related by the shear modulus, $G = c_{44} = 59 \text{ GPa}$ ¹, with $e_{ijk} = Gd_{ijk}$. For a cubic crystal with $\bar{4}3m$ symmetry with the primary axes, most of the

elements disappear leaving only the elements with indices ijk equal to a permutation of 123⁶. Each of these elements is equal to $\frac{1}{2}d_{14}$, which in GaAs and consequently our assumed isotropic semiconductor is $d_{14} = -2.69 \times 10^{-12} \text{ mV}^{-1}$.¹ The corresponding value for the strain piezoelectric tensor is given by $e_{14} = Gd_{14} = -0.16 \text{ Cm}^{-2}$.¹ For other orientations the piezoelectric tensor has to be rotated. If the gates are not aligned with the crystal axes the piezoelectric tensor must be rotated by $d'_{ijt} = R_{il}^{ca} R_{jm}^{ca} R_{kn}^{ca} d'_{lmn}$. This is accomplished by a rotation of θ about the z -axis. The rotation tensor necessary for this is

$$R^{ca} = \begin{pmatrix} \cos\theta & -\sin\theta & 0 \\ \sin\theta & \cos\theta & 0 \\ 0 & 0 & 1 \end{pmatrix}. \quad (2.5)$$

Due to the symmetry of the piezoelectric tensors, not only does the polarisation change with angle but also according to the surface on which the semiconductor has been grown. The rotation matrices for the surfaces I considered are

$$R_{ij}^{(110)} = \frac{1}{\sqrt{2}} \begin{pmatrix} \sqrt{2} & 0 & 0 \\ 0 & 1 & -1 \\ 0 & 1 & 1 \end{pmatrix}$$

$$R_{ij}^{(111)} = \frac{1}{\sqrt{6}} \begin{pmatrix} \sqrt{3} & -\sqrt{3} & 0 \\ 1 & 1 & -2 \\ \sqrt{2} & \sqrt{2} & \sqrt{2} \end{pmatrix} \quad (2.6)$$

$$R_{ij}^{(311)} = \frac{1}{\sqrt{22}} \begin{pmatrix} \sqrt{11} & -\sqrt{11} & 0 \\ 3 & 3 & -2 \\ \sqrt{2} & \sqrt{2} & 3\sqrt{2} \end{pmatrix}.$$

These rotations to the correct surfaces take place before the rotation of the z -axis, thus the fully transformed tensor d'_{ijk} for the new surface is given by

$$d'_{ijk} = R_{il}^{ca} R_{jm}^{ca} R_{kn}^{ca} R_{lo}^s R_{mp}^s R_{nq}^s d'_{opq}, \quad (2.7)$$

where R_{ij}^s is the rotation matrix for the new surface.

It is more convenient to work with the charge density ρ produced rather than the polarisation. This is given by

$$\rho = -\nabla \cdot \mathbf{P} = -d_{ijk} \frac{\partial}{\partial R_j} \sigma_{jk}, \quad (2.8)$$

where \mathbf{R} is a three-dimensional vector given by $\mathbf{R} = (x, y, z)$.

2.4 Electrical model

Again, the semiconductor is considered to be homogeneous with regard to electrical properties as well as elastic ones. Thus, the dielectric and piezoelectric constants are assumed to be the same throughout the material. This is a reasonable approximation as the values in GaAs and AlGaAs are similar. The dielectric constant ϵ_r is taken as $\epsilon_r = 13$.¹

The piezoelectric potential is assumed to have developed slowly, as the sample is cooled, so that the electrons in the 2DEG and the surface states have time to come to equilibrium. Therefore, the Fermi level can be considered to be pinned with the electrons free to move between the surface states and the 2DEG to maintain the Fermi Energy on the surface. Therefore, the surface can be treated as an equipotential¹².

There are two alternative approximations for a mobile charge around the donors. Sometimes there is a parasitic channel of electrons that remain free or very loosely bound even at low temperatures, but usually they are trapped in DX centres as the sample is cooled. However, even in these cases, the occupation is not random and some screening occurs. The two extreme models are either to ignore these electrons completely or to assume that the screening is so good the donor layer can be treated as an equipotential plane¹⁴.

The potential is calculated from the charge density using Poisson's equation

$$\nabla^2 \phi_{\text{bare}} = -\frac{\rho}{\epsilon_0 \epsilon_r}. \quad (2.9)$$

The boundary conditions for a two-dimensional potential are

$$\begin{aligned} \phi &\rightarrow 0 \text{ as } x, z \rightarrow \infty \\ \phi(x, z=0) &= 0 \end{aligned} \quad (2.10)$$

This second boundary condition can be modified to allow for the presence of a parasitic layer of electrons around the donors, so that the potential vanishes on this plane instead of the surface. The modified boundary conditions would be

$$\begin{aligned}\phi &\rightarrow 0 \text{ as } x, z \rightarrow \infty \\ \phi(x, z = d) &= 0\end{aligned}\tag{2.11}$$

where d is the depth of the donor layer. It is trivial to extend these boundary conditions to those for an island gate where the potential is three-dimensional and tends to zero as the y coordinate tends to infinity as well as x and z .

This potential however, does not take account of the 2DEG and the effect it has on the potential by redistributing itself in response to the applied potential. This is taken care of by screening using a Thomas-Fermi dielectric function³⁵, modified to allow for the nearest equipotential plane³.

$$\epsilon_{\text{TF}}(q, p) = 1 + \frac{2}{a_B q} [1 - \exp(-2pq)]\tag{2.12}$$

where p is the depth of the nearest equipotential plane and the Bohr Radius a_B is given by $a_B = 10 \text{ nm}$ for this system.¹ This screening takes place in Fourier space, however it can be approximated in real space by the d/dz approximation, details of which are given in §3.3.

The notation \tilde{A} is used for the Fourier transform of a quantity A throughout this document. Also ϕ is used for potentials and V is used for potential energies.

2.5 Deformation potential

In addition to the piezoelectric effect, the strain also interacts with the electrons through the deformation potential¹². While the piezoelectric potential remains the same if the carriers are holes, the deformation potential given here is only for electrons, the case for holes is more complicated. For electrons, the stress causes the edges of the energy bands to shift up or down proportionally to the dilation¹², δ given by⁵

$$\delta = \epsilon_{xx} + \epsilon_{yy} + \epsilon_{zz}.\tag{2.13}$$

Using the standard elastic equations [Eq. (2.2)], this can be expressed in terms of the stress as

$$\delta = \frac{1-2\nu}{E}(\sigma_{xx} + \sigma_{yy} + \sigma_{zz}) \quad (2.14)$$

The constant of proportionality is the deformation potential energy constant Ξ , so that the deformation potential energy is given by

$$V_{\text{def}} = \Xi\delta = \Xi(\varepsilon_{xx} + \varepsilon_{yy} + \varepsilon_{zz}) = \Xi \frac{1-2\nu}{E}(\sigma_{xx} + \sigma_{yy} + \sigma_{zz}). \quad (2.15)$$

The value for Ξ is assumed to be that for GaAs, $\Xi = -8 \text{ eV}$.¹ The deformation potential energy can also be screened using a Thomas Fermi dielectric function.

3 Single Stripe Gate

Larkin et. al.⁸ calculated the piezoelectric potential arising from a stripe gate on (100), and an array of such gates, in Fourier space. However, while this is good for an array of gates it is desirable to have a simple expression for the potential from a single gate in real space, due to the high number of Fourier components involved. I have therefore calculated this simple expression in real space. I have also extended these results to consider other surfaces for the gate as well as the [100] case. The 'stripe gates' considered here are rectangular gates whose length is much greater than their width so they can be considered infinitely long. Therefore these gates have one defining parameter, the width of the gate, and are therefore sometimes referred to as 1 dimensional gates.

3.1 Strain field

The Elastic models considered here are those given by Larkin et. al.⁸, I will briefly review them here.

The elastic gate is the limit of a thin gate, such that the lattice constant in the gate is forced to match that of the underlying substrate. Thus the gate is in constant stress, and exerts a force along the edges of the gate.

The rigid gate is the limit of a thick gate, such that the lattice constant in the substrate, directly beneath the gate, is forced to match that of the gate, while the lattice constant elsewhere on the surface is unaffected. Thus, the surface of the substrate is in constant stress underneath the gate.

Since we have assumed that there are no forces normal to the surface acting and consequently no bending, therefore we have plane strain which is defined by⁸

$$\epsilon_{yy} = \epsilon_{xy} = \epsilon_{yz} = 0, \sigma_{xy} = \sigma_{yz} = 0 \text{ and } \sigma_{yy} = \nu(\sigma_{xx} + \sigma_{zz}) \quad (3.1)$$

Using (3.1) to eliminate σ_{yy} from the standard relations between normal stress and strain [Eq. (2.2)] gives

$$\begin{aligned}
E\varepsilon_{xx}(x,|z|) &= (1-\nu^2)\sigma_{xx}(x,|z|) - \nu(1+\nu)\sigma_{zz}(x,|z|) \\
E\varepsilon_{zz}(x,|z|) &= (1-\nu^2)\sigma_{zz}(x,|z|) - \nu(1+\nu)\sigma_{xx}(x,|z|)
\end{aligned}
\tag{3.2}$$

where E is Young's modulus and ν is Poisson's ratio for the semiconductor.

Since we are considering the case of a thin gate, it is reasonable to consider that the stress and strain are independent of z throughout the thickness of the gate. Therefore since $\sigma_{zz}^{\text{gate}} = 0$, this is held throughout the gate. The normal stress and strain along x , the length of the gate are then related by $E_{\text{gate}}\varepsilon_{xx}^{\text{gate}}(x) = (1-\nu_{\text{gate}}^2)\sigma_{xx}^{\text{gate}}(x)$.

The relation between stress and applied force is $\mathbf{F} = -\text{div}\sigma$ with a body force \mathbf{F} per unit volume. On a surface, this becomes $\mathbf{P} = \sigma \cdot \hat{\mathbf{n}}$ where \mathbf{P} is the force per unit area and $\hat{\mathbf{n}}$ is an outward unit normal. On the exposed surface of the semiconductor, between the gates where no force is applied this gives $\sigma_{xz} = \sigma_{zx} = 0$. We have assumed that $\sigma_{zz}^{\text{gate}} = 0$ because the gate is thin and therefore $\sigma_{zz} = 0$ holds over the whole of the surface of the semiconductor.

The remaining stress $\sigma_{xx}^{\text{gate}}$ in the gate exerts a force per unit area $P_x(x)$ on the semiconductor underneath. Assuming a constant stress in the gate through the thickness h of the gate, the body force integrates to $P_x(x) = h d\sigma_{xx}^{\text{gate}}/dx$ (since the force is exerted by the gate on the semiconductor). This generates a shear stress on the semiconductor given by $\sigma_{xz}(x, z=0) = -P_x(x)$, on the surface. Thus, the stresses in the gate and semiconductor are related by

$$\sigma_{xz}(x, z=0) = -P_x(x) = -h \frac{d\sigma_{xx}^{\text{gate}}}{dx}.
\tag{3.3}$$

According to standard elastic theory⁵, the two-dimensional stress can be deduced from a biharmonic Airy stress function χ defined by

$$\nabla^4 \chi = 0,
\tag{3.4}$$

as follows

$$\sigma_{xx} = \frac{\partial^2 \chi}{\partial |z|^2}, \quad \sigma_{xz} = -\frac{\partial^2 \chi}{\partial x \partial |z|}, \quad \sigma_{zz} = \frac{\partial^2 \chi}{\partial x^2}, \quad \sigma_{yy} = \nu(\sigma_{xx} + \sigma_{zz}). \quad (3.5)$$

Because the system is in plane strain, the biharmonic potential χ can then be written as $\chi = |z|\varphi$ where $\nabla^2 \varphi = 0$. It is convenient when calculating the elastic potential to choose φ to be the imaginary part of a complex potential³ $\omega = \xi + i\varphi$, which is a function of the complex coordinate $\zeta = x + i|z|$. The stress in the semiconductor is given by

$$\begin{aligned} \sigma_{xx}(x, |z|) &= \frac{\partial^2(|z|\varphi)}{\partial |z|^2} = 2\frac{\partial \varphi}{\partial |z|} + z\frac{\partial^2 \varphi}{\partial |z|^2} = 2\text{Re}(\omega') - |z|\text{Im}(\omega''), \\ \sigma_{xz}(x, |z|) &= -\frac{\partial^2(|z|\varphi)}{\partial x \partial |z|} = -\frac{\partial \varphi}{\partial x} - |z|\frac{\partial^2 \varphi}{\partial x \partial |z|} = -\text{Im}(\omega') - |z|\text{Re}(\omega''), \\ \sigma_{zz}(x, z) &= \frac{\partial^2(|z|\varphi)}{\partial x^2} = |z|\frac{\partial^2 \varphi}{\partial x^2} = |z|\text{Im}(\omega''), \end{aligned} \quad (3.6)$$

where derivatives of ω are taken with respect to the complex variable ζ . Thus, it only remains to calculate $\omega(\zeta)$ for the different models of gate.

Taking the limit of $b \rightarrow \infty$ using $\lim_{\sin x \rightarrow 0} \sin x = x$ in Eq. (2.16) in Larkin et. al.⁸

$$\omega(\zeta) = -\frac{F_x^0}{\pi} \ln \frac{\sin \frac{1}{2}(Z - A)}{\sin \frac{1}{2}(Z + A)} \quad (3.7)$$

where $Z = \pi\zeta/(a+b)$ and $A = \pi a/(a+b)$, we obtain the function $\omega(\zeta)$ for a single elastic gate

$$\omega(\zeta) = -\frac{F_x^0}{\pi} (\ln(\zeta - a) - \ln(\zeta + a)). \quad (3.8)$$

For a single rigid gate $\omega(\zeta)$ is obtained from Davies and Larkin³ Eq. (4.8)

$$\omega(\zeta) = \frac{1}{2}\sigma_{xx}^0 \left(\zeta - \sqrt{\zeta^2 - a^2} \right), \quad (3.9)$$

with the branch cut chosen so that $\text{Im}\sqrt{\zeta^2 - a^2} > 0$, on the positive y axis.

Since $\nabla^2 \omega, \varphi = 0$, their Fourier transforms are of the form

$$V(x, z) = \int \tilde{v}(q) \exp(-iqx) \exp(-q|z|) dq. \quad (3.10)$$

Therefore, taking derivatives by z is equivalent to multiplying the Fourier transform by $-q$, and taking derivatives by x is equivalent to multiplying by $-iq$. This will be used later when calculating arrays of gates or when exact Thomas Fermi screening is required.

3.2 Deformation potential

The deformation potential is proportional to the dilation, which is given by [Eq. (2.15)]

$$\delta = \varepsilon_{xx} + \varepsilon_{yy} + \varepsilon_{zz} = \frac{1-2\nu}{E} (\sigma_{xx} + \sigma_{yy} + \sigma_{zz}).$$

However $\varepsilon_{yy} = 0$ [Eq. (3.1)] and $\sigma_{yy} = \nu(\sigma_{xx} + \sigma_{zz})$ [Eq. (3.5)], for this system therefore

$$\delta = \varepsilon_{xx} + \varepsilon_{zz} = \frac{1-2\nu}{E} (1+\nu) (\sigma_{xx} + \sigma_{zz}). \quad (3.11)$$

Using the expressions for the stress in Eq. (3.6), the dilation is given by

$$\delta = \frac{1-2\nu}{E} (1+\nu) 2 \operatorname{Re}(\omega'). \quad (3.12)$$

To obtain the potential energy in the 2DEG this is multiplied by Ξ the deformation potential constant [Eq. (2.15)].

$$V_{\text{def}} = \Xi \delta = \frac{\Xi 2(1+\nu)(1-2\nu)}{E} \operatorname{Re}(\omega') \quad (3.13)$$

This can then be Fourier transformed and screened, using Thomas Fermi screening [Eq.(2.12)],

$$\tilde{V}_{\text{def}}(q_x, q_z) = \frac{\Xi 2(1+\nu)(1-2\nu)}{\varepsilon_{\text{TF}}(q, \rho) E} \operatorname{Re}(\tilde{\omega}'(q_x, q_z)). \quad (3.14)$$

However, the dielectric function ε_{TF} [Eq. (2.12)] can be approximated by the following expression

$$\varepsilon_{\text{TF approx}}^{-1}(q, \rho) = \frac{a_B q}{2}, \quad (3.15)$$

when $1/p \ll q \ll 1/a_B$, and $q \neq 0$. This approximation is good when the 2DEG is far from the equipotential plane.

Since φ and ξ , and consequently the real and imaginary parts of derivatives of ω are harmonic functions, their Fourier components decay with depth like $\exp(-q|z|)$. Multiplication by q is therefore equivalent to taking the derivative $-d/d|z|$. Therefore, the approximate inverse dielectric function $\epsilon_{TF}^{-1} \text{ approx}$ [Eq. (3.15)] can be written in real space as

$$\epsilon_{d/dz}^{-1} = -\frac{a_B}{2} \frac{\partial}{\partial |z|}. \quad (3.16)$$

This gives the screened deformation potential as

$$V_{\text{def}} = \frac{\Xi(1+\nu)(1-2\nu)a_B}{E} \text{Im}(\omega^*). \quad (3.17)$$

I have therefore found a method for calculating an approximation to the screened deformation potential in real space.

Unlike the piezoelectric potential (§3.3-3.4), the dilation and consequently the deformation potential do not depend on orientation.

3.3 Piezoelectric potential on [100]

Larkin et al.⁸ calculated the potential arising from an array of gates (an LSSL) through the Fourier transform of the potential. While this only needs a few Fourier components, the single gate requires many more. It is therefore desirable to have an expression for the potential in real space.

The charge density is given by [Eq. (2.8)]

$$\rho = d_{ijk} \frac{\partial}{\partial r_l} \sigma_{jk}.$$

For the (100) surface this works out to

$$\rho = d_{14} \sin 2\theta \left(\frac{\partial}{\partial x} \sigma_{xz} + \frac{1}{2} \frac{\partial}{\partial |z|} \sigma_{xx} - \frac{1}{2} \frac{\partial}{\partial |z|} \sigma_{yy} \right). \quad (3.18)$$

Using Eq. (3.5) to eliminate σ_{yy}

$$\rho = \frac{1}{2} d_{14} \sin 2\theta \left(2 \frac{\partial}{\partial x} \sigma_{xz} + (1-\nu) \frac{\partial}{\partial |z|} \sigma_{xx} - \nu \frac{\partial}{\partial |z|} \sigma_{zz} \right), \quad (3.19)$$

and then substituting derivatives of φ for σ_{ij} from Eq. (3.6) gives

$$\rho = \frac{1}{2} d_{14} \sin 2\theta \left[(-2-\nu) \frac{\partial^2 \varphi}{\partial x^2} + 3(1-\nu) \frac{\partial^2 \varphi}{\partial |z|^2} + (-2-\nu) z \frac{\partial^3 \varphi}{\partial x^2 \partial |z|} + (1-\nu) z \frac{\partial^3 \varphi}{\partial |z|^3} \right] \quad (3.20)$$

Since φ is a harmonic function $\frac{\partial^2 \varphi}{\partial x^2} = -\frac{\partial^2 \varphi}{\partial |z|^2}$. Thus allowing us to simplify this

expression to

$$\rho = \frac{1}{2} d_{14} \sin 2\theta \left[(5-2\nu) \frac{\partial^2 \varphi}{\partial |z|^2} + 3z \frac{\partial^3 \varphi}{\partial |z|^3} \right]. \quad (3.21)$$

This can be expressed simply in terms of $\omega(\zeta)$

$$\rho = -\frac{1}{2} d_{14} \sin 2\theta [(5-2\nu) \text{Im}(\omega'') + 3z \text{Re}(\omega''')]. \quad (3.22)$$

This is equivalent to the result by Asbeck et. al.³³ for the charge density under a gate aligned along $[01\bar{1}]$ on (100)

$$\rho = \gamma_b \sigma_f d_f \left(\frac{x_1 z (x_1^2 - \beta z^2)}{r_1^6} - \frac{x_2 z (x_2^2 - \beta z^2)}{r_2^6} \right), \quad (3.23)$$

where $\gamma_b = 2d_{14}(4+\nu)/\pi$, $x_1 = x-a$, $r_1 = \sqrt{x_1^2 + z^2}$, $x_2 = x+a$, $r_2 = \sqrt{x_2^2 + z^2}$, $\beta = (2+\nu)/(4+\nu)$, σ_f is the tensile stress in the gate and d_f is the thickness of the gate.

To get the potential, Poisson's equation [Eq. (2.9)]

$$\nabla^2 \phi_{\text{barr}} = -\frac{\rho}{\epsilon_0 \epsilon_r}$$

needs to be solved. The boundary conditions I have used are those given by Eq. (2.9), for no parasitic layer.

$$\phi \rightarrow 0 \text{ as } x, z \rightarrow \infty$$

$$\phi(x, z = 0) = 0$$

I have solved Poisson's equation by assuming the form of the potential to be

$$\phi = A|z|\text{Re}(\omega') + B|z|^2 \text{Im}(\omega') + C|z|\text{Re}(\omega'') + D|z|^2 \text{Im}(\omega''), \quad (3.24)$$

and then substituting this into Poisson's equation to find the constants. This gives

$$\phi_{\text{bare}} = \frac{d_{14}}{8\epsilon_0\epsilon_r} \sin 2\theta \left[(7 - 4\nu)|z|\text{Re}(\omega') - 3|z|^2 \text{Im}(\omega'') \right]. \quad (3.25)$$

This can be Fourier transformed in x and $|z|$ to allow us to calculate the screened potential. The d/dz approximation to screening, discussed in §3.2, cannot be directly applied since ϕ_{bare} is not a harmonic function. However, it is noticed that

$$\phi_{\text{bare}} = \sum_i A_i |z|^i H_i, \quad (3.26)$$

where the H_i are harmonic functions and the A_i are constants. Therefore the approximate inverse dielectric function $\epsilon_{d/dz}^{-1}$ [Eq. (3.16)] can be applied just to the harmonic parts of the potential. So that for the general potential expressed in Eq. (3.26), the screened potential is given by

$$\phi = \sum_i A_i |z|^i \epsilon_{d/dz}^{-1} H_i. \quad (3.27)$$

Using this expression, we can obtain the following expression for the approximate screened potential energy in the 2DEG

$$V = -\frac{ed_{14}a_B}{16\epsilon_0\epsilon_r} \sin 2\theta \left[(7 - 4\nu)|z|\text{Im}(\omega'') + 3|z|^2 \text{Re}(\omega''') \right] \quad (3.28)$$

where $-e$ is the electronic charge. This approximation can also be applied to the deformation potential.

Thus we have a simple expression in real space that is an approximation to the screened potential energy in the 2DEG.

3.4 Piezoelectric potential on different surfaces

Using the rotation matrices in Eq. (2.6) to rotate the piezoelectric tensor d_{ijk} for some common surfaces [(110),(111),(311)³⁶] it is possible to calculate the charge densities for gates on these surfaces using Eq. (2.8)

$$\rho = d_{ijk} \frac{\partial}{\partial r_i} \sigma_{jk},$$

in terms of derivatives of the stress σ_{ij} . These are

$$\rho_{110} = \frac{1}{8} d_{14} \left[\left(8 \frac{\partial}{\partial |z|} \sigma_{xz} + \frac{\partial}{\partial x} (4\sigma_{zz} - 3\sigma_{xx} - \sigma_{yy}) \right) \cos \theta + 3 \frac{\partial}{\partial x} (\sigma_{xx} - \sigma_{yy}) \cos 3\theta \right] \quad (3.29)$$

$$\rho_{111} = \frac{d_{14}}{2\sqrt{3}} \left[\frac{\partial}{\partial x} (\sigma_{xx} + \sigma_{yy} - 2\sigma_{zz}) + 2 \frac{\partial}{\partial x} \sigma_{xz} + \sqrt{2} \frac{\partial}{\partial x} (\sigma_{yy} - \sigma_{xx}) \sin 3\theta \right] \quad (3.30)$$

$$\begin{aligned} \rho_{311} = \frac{d_{14}}{22\sqrt{11}} & \left[9 \frac{\partial}{\partial |z|} (\sigma_{xx} + \sigma_{yy} - 2\sigma_{zz}) + 2 \frac{\partial}{\partial x} \sigma_{xz} \right. \\ & + 2\sqrt{2} \left(16 \frac{\partial}{\partial |z|} \sigma_{xz} + \frac{\partial}{\partial x} (6\sigma_{xx} + 2\sigma_{yy} - 8\sigma_{zz}) \right) \sin \theta \\ & + 24 \left(\frac{\partial}{\partial |z|} (\sigma_{xx} - \sigma_{yy}) + 2 \frac{\partial}{\partial x} \sigma_{xz} \right) \cos 2\theta \\ & \left. + 15\sqrt{2} \frac{\partial}{\partial x} (\sigma_{yy} - \sigma_{xx}) \sin 3\theta \right] \quad (3.31) \end{aligned}$$

which in terms of derivatives of $\omega(\zeta)$ are

$$\rho_{110} = -\frac{1}{8} d_{14} \left[(2(1+\nu) \operatorname{Re}[\omega''] - 15|z| \operatorname{Im}[\omega''']) \cos \theta + (6(\nu-1) \operatorname{Re}[\omega''] + 3|z| \operatorname{Im}[\omega''']) \cos 3\theta \right] \quad (3.32)$$

$$\rho_{111} = -\frac{d_{14}}{2\sqrt{3}} \left[(7+2\nu) \operatorname{Im}[\omega''] + 5|z| \operatorname{Re}[\omega'''] - \sqrt{2} (2(\nu-1) \operatorname{Re}[\omega''] + |z| \operatorname{Im}[\omega''']) \sin 3\theta \right] \quad (3.33)$$

$$\begin{aligned}
\rho_{311} = & \frac{d_{14}}{22\sqrt{11}} \left[-9(7+2\nu)\text{Im}[\omega''] - 45|z|\text{Re}[\omega''] \right. \\
& + 4\left(2(1+\nu)\text{Re}[\omega''] - 15\sqrt{2}|z|\text{Im}[\omega'']\right)\sin\theta \\
& + 24\left((2\nu-5)\text{Im}[\omega''] + 3|z|\text{Re}[\omega'']\right)\cos 2\theta \\
& \left. + 15\left(2(\nu-1)\text{Re}[\omega''] + \sqrt{2}|z|\text{Im}[\omega'']\right)\sin 3\theta \right]
\end{aligned} \tag{3.34}$$

The bare potential can be found by solving Poisson's equation [Eq. (2.9)] using the same technique as in §3.3. I assumed the same form for the solution [Eq. (3.24)]

$$\phi = A|z|\text{Re}(\omega') + B|z|^2 \text{Im}(\omega') + C|z|\text{Re}(\omega'') + D|z|^2 \text{Im}(\omega'')$$

and then substituting this back into Poisson's equation to work out the constants. The bare potentials for these surfaces are given by

$$\begin{aligned}
\phi_{\text{bare}}^{110} = & -\frac{d_{14}}{32\varepsilon_0\varepsilon_r\varepsilon_{yy}(g_{ii})}|z|\left[\left((29+4\nu)\text{Im}[\omega'] + 15|z|\text{Re}[\omega'']\right)\cos\theta \right. \\
& \left. + \left(3(4\nu-3)\text{Im}[\omega'] - 3|z|\text{Re}[\omega'']\right)\cos 3\theta \right]
\end{aligned} \tag{3.35}$$

$$\begin{aligned}
\phi_{\text{bare}}^{111} = & -\frac{d_{14}}{8\sqrt{3}\varepsilon_0\varepsilon_r}|z|\left[\left(9+4\nu\right)\text{Re}[\omega'] - 5|z|\text{Im}[\omega''] \right. \\
& \left. + \sqrt{2}\left(\left(4-3\nu\right)\text{Im}[\omega'] - |z|\text{Re}[\omega'']\right)\sin 3\theta \right]
\end{aligned} \tag{3.36}$$

$$\begin{aligned}
\phi_{\text{bare}}^{311} = & \frac{d_{14}}{88\sqrt{11}\varepsilon_0\varepsilon_r}|z|\left[3\left(12\nu+27\right)\text{Re}[\omega'] - 45|z|\text{Im}[\omega''] \right. \\
& + 4\left(\left(29+4\nu\right)\text{Im}[\omega'] + 15\sqrt{2}|z|\text{Re}[\omega'']\right)\sin\theta \\
& + 3\left(\left(56-32\nu\right)\text{Re}[\omega'] - 24|z|\text{Im}[\omega'']\right)\cos 2\theta \\
& \left. + 15\left(\left(4\nu-3\right)\text{Im}[\omega'] - \sqrt{2}|z|\text{Re}[\omega'']\right)\sin 3\theta \right]
\end{aligned} \tag{3.37}$$

And the approximate screened potential energies in the 2DEGs, given by the d/dz approximation to Thomas Fermi screening [Eq's (3.16) and (3.27)], are

$$\begin{aligned}
V_{110} = & \frac{ed_{14}a_B}{64\varepsilon_0\varepsilon_r}|z|\left[\left(\left(29+4\nu\right)\text{Re}[\omega''] - 15|z|\text{Im}[\omega''']\right)\cos\theta \right. \\
& \left. + \left(3\left(4\nu-3\right)\text{Re}[\omega''] + 3|z|\text{Im}[\omega''']\right)\cos 3\theta \right]
\end{aligned} \tag{3.38}$$

$$\begin{aligned}
V_{111} = & -\frac{ed_{14}a_B}{16\sqrt{3}\varepsilon_0\varepsilon_r}|z|\left[\left(9+4\nu\right)\text{Im}[\omega''] + 5|z|\text{Re}[\omega'''] \right. \\
& \left. - \sqrt{2}\left(\left(4-3\nu\right)\text{Re}[\omega''] + |z|\text{Im}[\omega''']\right)\sin 3\theta \right]
\end{aligned} \tag{3.39}$$

$$\begin{aligned}
V_{311} = & -\frac{ed_{14}a_B}{176\sqrt{11}\epsilon_0\epsilon_r}|z|\left[-3(12\nu+27)\text{Im}[\omega'']-45|z|\text{Re}[\omega''']\right. \\
& +4\left((29+4\nu)\text{Re}[\omega'']-15\sqrt{2}|z|\text{Im}[\omega''']\right)\sin\theta \\
& -3\left((56-32\nu)\text{Im}[\omega'']-24|z|\text{Re}[\omega''']\right)\cos 2\theta \\
& \left.+15\left((4\nu-3)\text{Re}[\omega'']+\sqrt{2}|z|\text{Im}[\omega''']\right)\sin 3\theta\right]
\end{aligned} \tag{3.40}$$

3.5 Results

The piezoelectric potential on (100) is even in x , and varies as $\sin 2\theta$ with angle θ from (010). The potential therefore reaches a maximum when aligned with the cleavage planes (011), at 45° to the crystal axes. The piezoelectric potential vanishes for gates aligned along the cleavage planes, although the deformation potential, which does not vary with orientation, is still present.

The piezoelectric potential on (110) is odd in x and has two components which vary with angle, one proportional to $\cos \theta$ and one proportional to $\cos 3\theta$. The $\cos \theta$ term dominates. The potential reaches a maximum when the gate is aligned to the crystal axis (010). Unlike (100), there is no orientation of gate for which the piezoelectric potential vanishes.

On (111) the piezoelectric potential again has two components, a dominant even component, which is isotropic and a smaller odd component, approximately one third the size, with an angular dependence of $\sin 3\theta$.

On (311) there are four components. The first is isotropic and even, while the second is also even but with an angular dependence of $\cos 2\theta$. The two odd components have angular dependencies of $\sin \theta$ and $\sin 3\theta$.

The potential energy for the different orientations on the different substrates is shown in Figure 9 along with the deformation potential, which is the same on all surfaces, with these approximations, for comparison.

For a gate aligned with the cleavage planes on the (100) surface the ratio between the deformation potential energy and the piezoelectric potential energy is given by

$$\frac{V_{\text{piezo}}}{V_{\text{def}}} = \frac{ed_{14}E}{\varepsilon 16\varepsilon_0\varepsilon_r(1+\nu)(1-2\nu)} |z| \left[(7-4\nu) + \frac{3|z|\text{Re}(\omega'')}{\text{Im}(\omega'')} \right]. \quad (3.41)$$

Thus the deformation becomes more important the nearer the 2DEG is to the surface, and it also depends on the elastic model used. The ratio between the potential energies works out at around 10 for the surfaces considered here.

The different approximations to the screening are shown in Figure 10. The d/dz approximation is compared with the exact Thomas Fermi screening and a further approximation in which the exponential term is omitted, hereafter referred to as the no exponential approximation. The approximations have two effects on the screened potential energy. The magnitude of the potential is slightly reduced, in the d/dz approximation and the no exponential approximation. This is not very prominent in Figure 10, but when the depth of the 2DEG is reduced it becomes more prominent, with a reduction in magnitude of around 0.8 for the d/dz approximation when the depth is set to 25 nm. The oscillations under the edge of the gate are also increased. This is most marked in the d/dz approximation but also occurs in the no exponential approximation.

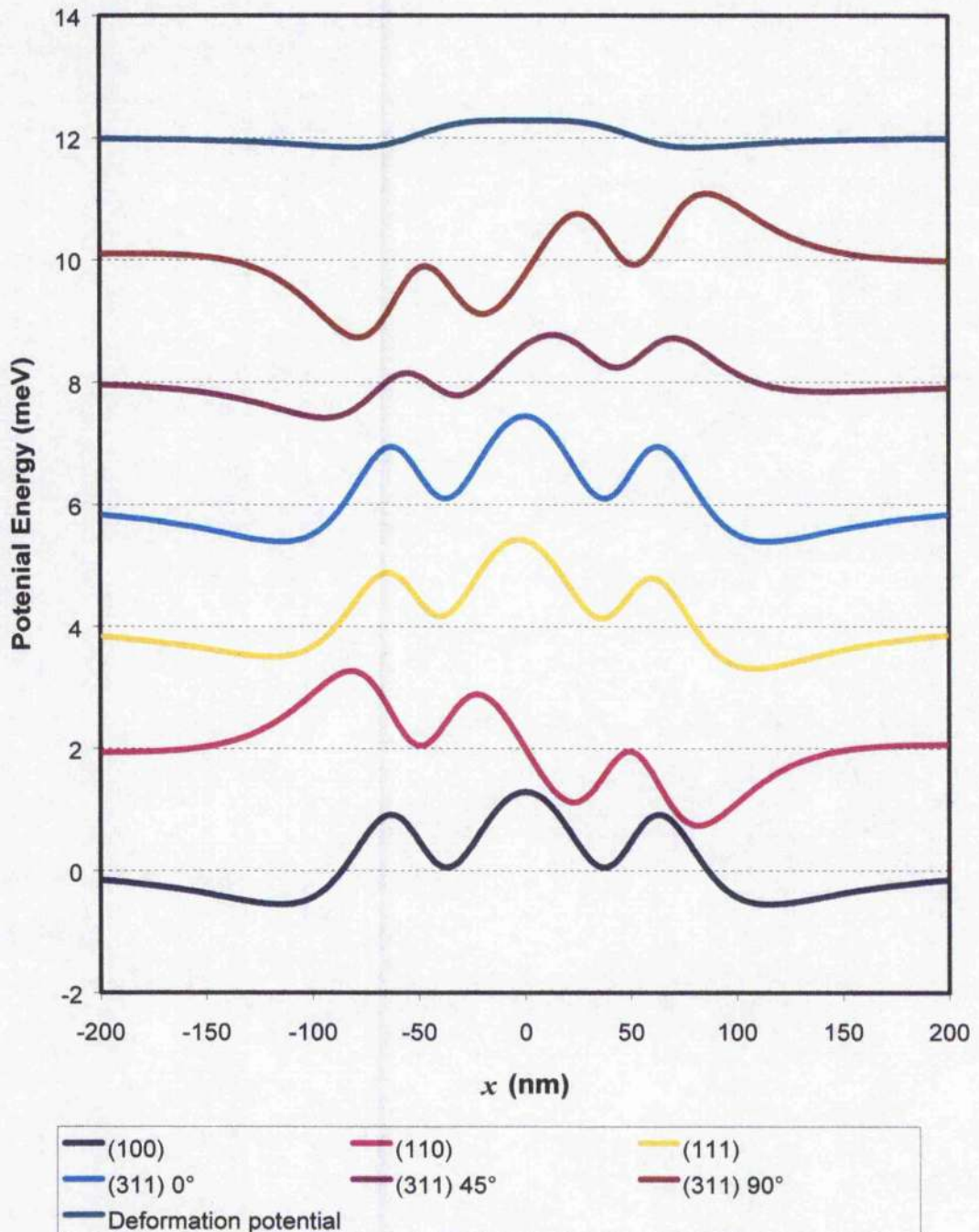


Figure 9 Screened piezoelectric potential energy in 2DEG's, at a depth of 50 nm with no parasitic layer, under stripe gates of width 100 nm on various surfaces. Curves are offset for clarity with the corresponding zero's shown as dashed lines. The deformation potential energy is also shown for comparison.

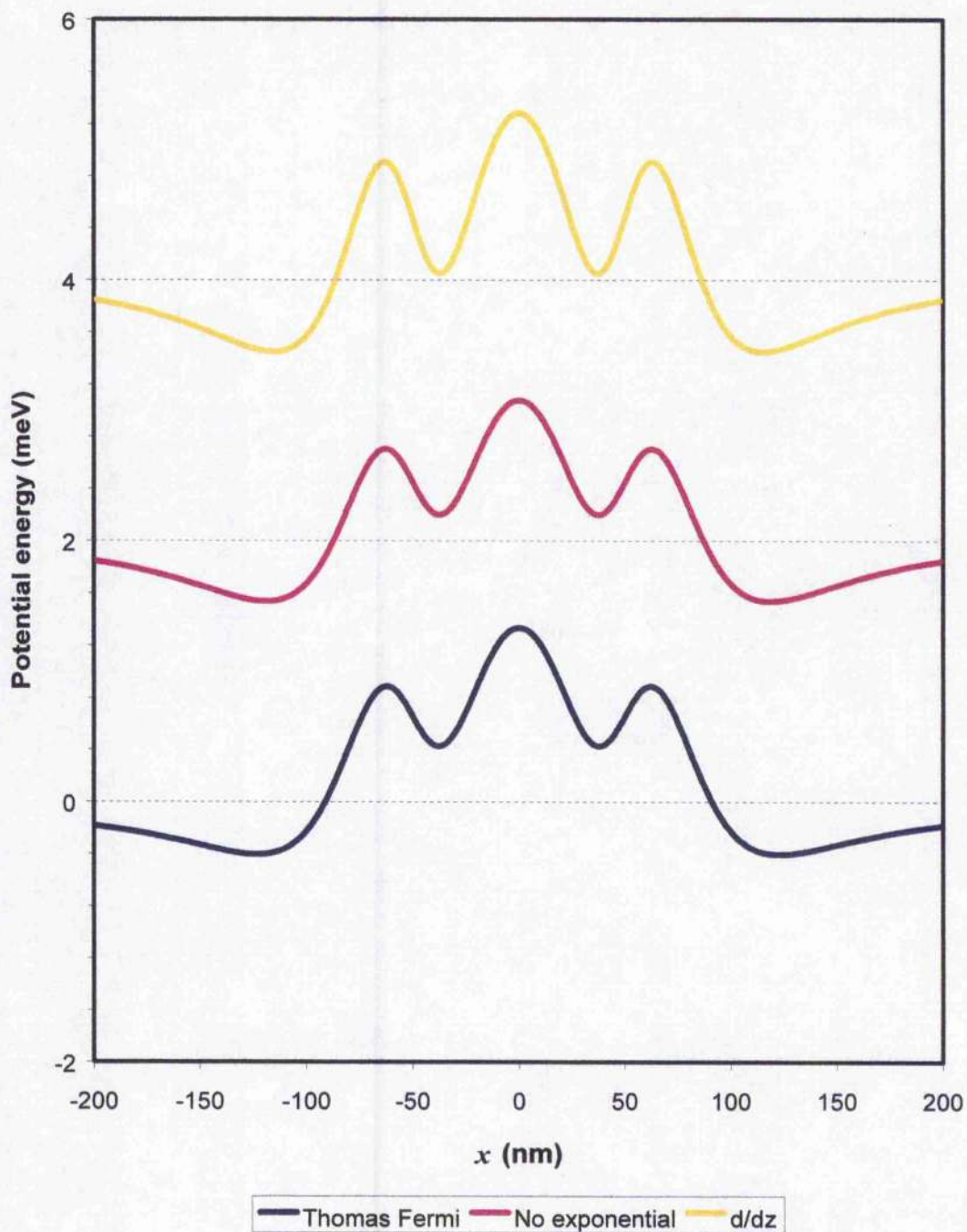


Figure 10 Approximations to the screened piezoelectric potential energy in a 2DEG, at a depth of 50 nm with no parasitic layer, under a stripe gate of width 100 nm. Curves are offset for clarity with the corresponding zero's shown as dashed. The d/dz approximation is shown along with the exact Thomas Fermi screening and a further approximation where the exponential term is neglected in Thomas Fermi screening.

3.6 Conclusions

I have calculated expressions in real space for the piezoelectric potential energies and the deformation potential energy in a 2DEG below a stripe gate on the (100), (110), (111) and (311) surfaces. I have also provided a method for the calculation of these potential energies on any surface given a rotation matrix, that rotates the (100) axis to the defining direction in the perpendicular to the chosen surface.

The d/dz real space approximation to Thomas Fermi screening is not perfect and results in distortions of the oscillations under the edges of the gate. However, the gains in speed and ease of calculation are in my opinion worth this loss of accuracy where only a rough calculation is needed, since the Fourier transform can be avoided.

If it is desirable to avoid the piezoelectric potential under the gate experimentally then this can be achieved on (100) if the gate is aligned to the crystal axes. However, the deformation potential which is isotropic will remain. The deformation potential is approximately a factor of 10 smaller though. This avoidance is not possible with any of the other surfaces considered here. If the piezoelectric potential is to be harnessed, then the effect can be maximised by choosing the orientation of the device. On (100), the gate should be aligned with the cleavage planes. However, the effect can be increased even more if a different surface can be chosen. The largest effect is from the (111) surface.

The size of the potentials is around 1 meV for a metal gate, and several times this and up to at least 10 meV if strained layers are used.

If a metal gate is used and a voltage is applied to the gate, then the potential produced in the 2DEG will be an even function and will combine with the potential produced from the piezoelectric effect. Either potential can be used to enhance the potential or to reduce it. However, this method cannot be used to eliminate the built in potential since the shape of the potentials will be different.

The unexpected nature of the potentials under the edge of the gate can be explained trivially with reference to the method of calculation discussed in §5. It can be seen from Figure 15, that if the gate is modelled as two forces at either side of the gate then the overlapping structure of the charge densities produced from two point forces would look like that shown in Figure 9. It should also be noted that this effect is somewhat enhanced by the approximations involved in d/dz screening.

Since the results I have presented are in real space, they are useful for quick calculations of an estimate of the potential under a single gate. While they are not as accurate as an inverse Fourier transform of the correctly screened version as presented in Larkin et. al.⁸, they are a lot quicker to calculate, since even fast Fourier transforms (FFTs) require a large amount of computer time to calculate.

The effect on FETs can also be calculated from my results. These results demonstrate the need to include strain effects, particularly the piezoelectric effect when modelling devices. In this case, it should be straightforward to include the potentials as presented here in models for all types of FET. The screened potential should be used for MODFETs and the bare potential for other types of FET without a 2DEG. However, some effects can be calculated more directly, e.g. the shift in the threshold voltage. This can be calculated by simply adding the maximum of the bare potential to the threshold voltage calculated neglecting strain. The bare potential should be used even for MODFETs since the threshold voltage is when the channel is completely depleted and therefore the 2DEG is not present and cannot screen.

4 One-dimensional Lateral Surface Superlattices

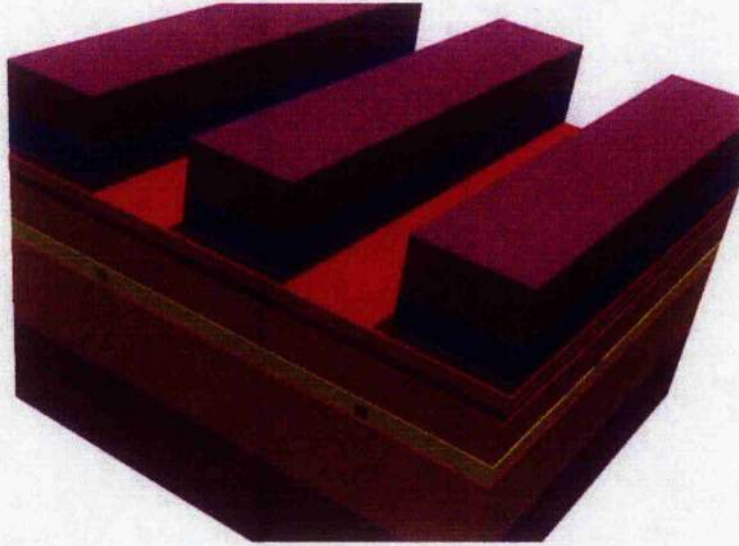


Figure 11 A section of a one-dimensional LSSL, made by etching InGaAs layers. Purple - GaAs, Red - AlGaAs, Yellow - Delta doped AlGaAs, Blue - InGaAs.

4.1 Extension to Lateral Surface Superlattices

It is straightforward to extend the results for the Fourier transform of the potential produced by a single gate to that for an array of gates (a 1D LSSL), as shown in Figure 11. For a square array of gates aligned along the principle axis x , with period b , the Fourier transform, in x , of the potential for a single gate must be changed to a Fourier series. This is achieved by limiting the coefficients to the wave vectors of the reciprocal lattice and dividing the Fourier Transform by b .

$$V(x, z) = \frac{1}{b} \sum_n \tilde{V}(q_n) \exp(-iq_n x) \exp(-q_n |z|) \quad (4.1)$$

where $\tilde{V}(q)$ is the Fourier transform of the potential energy in the 2DEG. The reciprocal lattice vectors q_n are given by

$$q_n = \frac{2\pi}{b} n \quad (4.2)$$

Thus the Fourier coefficients of the bare potential energy of a 1D LSSL aligned to the crystal axis on a (100) surface are

$$\tilde{V}_{\text{bare}} = -\frac{ed_{14}}{8\varepsilon_0\varepsilon_r}|z|[(7-4\nu)\text{Re}(\tilde{\omega}_n')-3|z|\text{Im}(\tilde{\omega}_n'')]\sin 2\theta \quad (4.3)$$

where $\tilde{\omega}_n = \tilde{\omega}(q_n)$. This can be expressed in terms of derivatives of $\tilde{\varphi}$ instead,

$$\tilde{V}_{\text{bare}} = -\frac{ed_{14}}{8\varepsilon_0\varepsilon_r}|z|\left[(7-4\nu)\frac{\partial\tilde{\varphi}_n}{\partial|z|}+3|z|\frac{\partial^2\tilde{\varphi}_n}{\partial|z|^2}\right]\sin 2\theta \quad (4.4)$$

allowing the use of the trick discussed at the end of §3.1 to replace derivatives with multiplication by $-q_n$. The screened potential energy is therefore given by

$$\tilde{V}(q_n) = \frac{ed_{14}a_B}{16\varepsilon_0\varepsilon_r\varepsilon_{TF}(q_n)}q_n|z|\tilde{\varphi}_n[7-4\nu-3q_n|z|]\sin 2\theta, \quad (4.5)$$

which is consistent with Larkin et. al.⁸

The equivalent expressions for the other surfaces considered are

$$\tilde{V}_{110} = \frac{-ied_{14}q_n|z|\tilde{\varphi}_n}{32\varepsilon_0\varepsilon_r\varepsilon_{TF}(q_n)}\left[(29+4\nu-15q_n|z|)\cos\theta+(12\nu-9+3q_n|z|)\cos 3\theta\right] \quad (4.6)$$

$$\tilde{V}_{111} = \frac{-ed_{14}q_n|z|\tilde{\varphi}_n}{8\sqrt{3}\varepsilon_0\varepsilon_r\varepsilon_{TF}(q_n)}\left[9+4\nu-5q_n|z|+\sqrt{2}i(4-3\nu+q_n|z|)\sin 3\theta\right] \quad (4.7)$$

$$\tilde{V}_{311} = \frac{ed_{14}q_n|z|\tilde{\varphi}_n}{88\sqrt{11}\varepsilon_0\varepsilon_r\varepsilon_{TF}(q_n)}\left[36\nu+81-45q_n|z|+3(56-32\nu-24q_n|z|)\cos 2\theta\right. \\ \left.+i\left\{4(29+4\nu-15\sqrt{2}q_n|z|)\sin\theta+15(4\nu-3-\sqrt{2}q_n|z|)\sin 3\theta\right\}\right] \quad (4.8)$$

4.2 Comparison with experiments

Evidence for the dominance of the piezoelectric potential in LSSLs with metal gates at low gate voltage, has been produced by experiments carried out at Glasgow^{2,37}. Initial experiments showed that the orientation dependence of the potential was exactly of the form predicted by theory. The magnitude of the potential with the predicted theory is also in remarkable agreement. However, the harmonic content has not been so successful, with the harmonic content matching that of the deformation potential and not the piezoelectric potential. This lack of agreement can be attributed to the crude approximations in the elastic model and ignoring any bending in the gates

or forces perpendicular to the surface of the semiconductor. In this case, it would appear only a coincidence that the harmonic content matches that for the deformation potential for the elastic model.

These effects have also been seen in the deliberately strained layers grown in Glasgow^{4,7}. These layers include the addition of a InGaAs layer grown on top of a standard heterostructure [Figure 6] which is then etched to pattern the strain. However, a number of other effects have been raised, as can be seen from the magnetoresistance traces [Figure 12]. The effects can be summarised as

1. There are commensurability oscillations (COs) along the [001], [010] directions, where none should be expected if the effect is due entirely to the piezoelectric effect.
2. In the [011] direction, the COs are much more pronounced, reflecting a stronger potential modulation. None of the higher harmonics expected from the piezoelectric effect are observed in the magnetoresistance. However when the COs are Fourier transformed weak higher harmonics are observed.
3. In the $[01\bar{1}]$ direction the COs are smaller than in the other directions studied. Additional minima at 0.29 and 0.49 T show clearly the expected second harmonic but the magnitudes are larger than expected. When the COs are Fourier transformed the second harmonic is dominant with a weaker first harmonic.

These results are explained by the recognition that there is an additional potential in the system, due to the etching of the InGaAs. When the surface is etched, it brings the surface states closer to the 2DEG; this produces an effective positive potential under the areas etched. This effect is referred to as the surface potential and is estimated to be around 0.7 meV for this system⁴. This potential produces the COs in the control sample with no InGaAs and in the [001] and [010] directions where no piezoelectric potentials are present. In the piezoelectric directions, [011] and $[01\bar{1}]$, it is the interplay between the surface potential and the piezoelectric potential that produces the COs. In the [011] direction the surface potential and the fundamental component of the piezoelectric potential are of the same sign and combine to give a large potential that swamps the much smaller harmonics. In the $[01\bar{1}]$ direction the

fundamental piezoelectric component and the surface potential come close to cancelling each other, leaving the smaller second harmonic to dominate.

Similar experiments were carried out in München by Luyken et. al.³⁸. They, however, concluded that the COs were the result of the deformation potential, due to the harmonic content. These conclusions are disputed by Glasgow, particularly in the light of my calculations, which show that the piezoelectric potential should be dominant. Since the direction of the current is not given by Luyken et. al. it is difficult to compare results directly but, with the orientation agreement of the Glasgow samples and the difference in magnitudes mean that it is hard to believe that the deformation potential should be dominant.

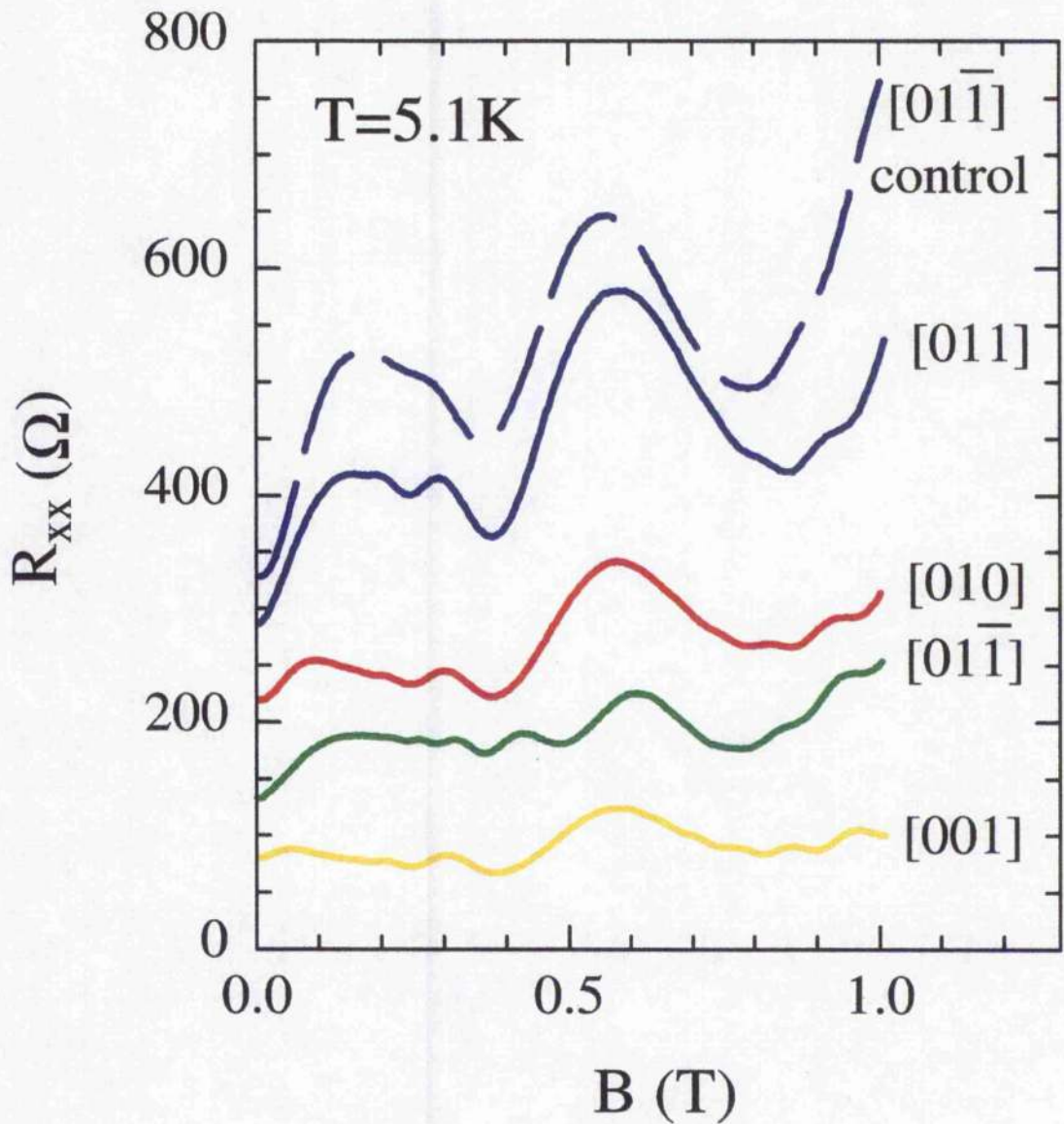


Figure 12 Magnetoresistance of four Hall bars with stressed superlattices of different orientations. Curves are offset for clarity as follows: $[01\bar{1}] + 50 \Omega$; $[010] + 100 \Omega$; and $[011] + 150 \Omega$. The temperature was 5.1 K to suppress Shubniko-de Haas oscillations. The strong dependence on orientation is a signature of the piezoelectric effect. The magnetoresistance of an unstressed $[01\bar{1}]$ control sample is shown by the dashed blue line and depends only weakly on orientation.

4.3 Conclusions

I have produced expression for the screened potential under a LSSL on some common surfaces (100), (110), (111) and (311). In the experiments conducted at Glasgow^{4,7}, the theory has been confirmed and the piezoelectric potential is dominant over the deformation potential.

An interesting effect that can be harnessed is that the sign of the Fourier components changes as the depth is varied. This allows tuning of the gate width and 2DEG depth, to null any given Fourier component. If this is used to null the fundamental component then the second harmonic dominates and the effective period of the superlattice is halved. This is extremely useful when the aim is to construct LSSLs with as small a period as possible to observe quantum effects. This effect can also be achieved by the interplay between the different sources of potential in the system, as in the experiments at Glasgow⁴.

5 Island Gates

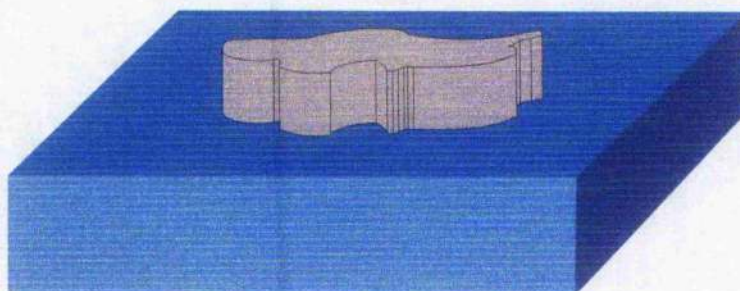


Figure 13 A general surface structure of the surface of a semiconductor

I have calculated the strain arising when an isolated square or circular gate is placed on the surface of a semiconductor and used this to calculate the deformation and piezoelectric potentials produced. I started by calculating the piezoelectric charge density and potentials, when feasible, in real space using the incompressible approximation and then moved to Fourier space for a more complete picture. Finding an elastic potential is more complicated in 3 dimensions than in 2, and I therefore abandoned this approach in favour of considering the potential from a single point force and building up the overall potential from this.

An island gate is defined to be any isolated structure on the surface of a semiconductor, as shown in Figure 13. This applies to traditional gates made by depositing metal on the surface or more exotic structures like etched InGaAs layers^{4,7}. Although some of these structures are strictly not gates, the term 'gate' is less unwieldy than the more general 'surface structure' and the structures are therefore referred to as 'gates' throughout this document. In principle, the methods discussed here will work for any such structure, however the cases explicitly considered here are regular shaped gates, either rectangular or circular.

5.1 Elastic model

I used the elastic model for the gate as described in §3.1. The gate is in constant stress. Thus, the gate exerts a force on the substrate around the perimeter of the gate and parallel to the surface of the semiconductor, as shown in Figure 14.



Figure 14 Some of the forces for the elastic model of gate.

We build up this elastic field from the Cerruti problem³⁴, of a single point force parallel to and on the surface of a semi-infinite elastic medium. In conformity with our chosen axes, the equations given here are for a medium with $z > 0$. The displacement is given for $z > 0$ by

$$\begin{aligned}
 u_x(\mathbf{r}) &= \frac{F_x}{4\pi G} \left\{ \frac{1}{R} + \frac{x^2}{R^3} + (1-2\nu) \left[\frac{1}{R+|z|} - \frac{x^2}{R(R+|z|)^2} \right] \right\}, \\
 u_y(\mathbf{r}) &= \frac{F_x}{4\pi G} \left[\frac{xy}{R^3} - (1-2\nu) \frac{xy}{R(R+|z|)^2} \right], \\
 u_z(\mathbf{r}) &= \frac{F_x}{4\pi G} \left[-\frac{x|z|}{R^3} - (1-2\nu) \frac{x}{R(R+|z|)^2} \right],
 \end{aligned} \tag{5.1}$$

where $R = \sqrt{x^2 + y^2 + z^2}$. This simplifies if the substrate is considered incompressible ($\nu = \frac{1}{2}$).

$$\begin{aligned}
 u_x^i(\mathbf{r}) &= \frac{F_x}{4\pi G} \left\{ \frac{1}{R} + \frac{x^2}{R^3} \right\}, \\
 u_y^i(\mathbf{r}) &= \frac{F_x}{4\pi G} \left[\frac{xy}{R^3} \right], \\
 u_z^i(\mathbf{r}) &= \frac{F_x}{4\pi G} \left[-\frac{x|z|}{R^3} \right].
 \end{aligned} \tag{5.2}$$

This allows some calculations to take place in real space. However in Fourier space, this approximation does not simplify the result. There is a singularity along the negative z -axis in the displacement, which is not a physical problem since this is outside the medium but it does prevent the Fourier transform from converging. Therefore the transform is carried out in x and y only leaving z in real space. This is convenient because this allows us to specify the depth of the 2DEG and the donors in real space.

The Fourier transform is done in two parts. Firstly, the incompressible part of the displacement is Fourier transformed and then we can add the part that depends on ν , which is tricky to Fourier transform. Using the relation

$$FT[xf(x)] = i \frac{FT[f(x)]}{q_x} \quad (5.3)$$

it is easiest if the Fourier transform is done in polar coordinates, $r = \sqrt{x^2 + y^2}$, ϕ which transform to $q = \sqrt{q_x^2 + q_y^2}$, q_ϕ . \mathbf{u}^i can be built up from Eq. (5.3) and Fourier transforms of $\frac{r}{R}$ and $\frac{r}{R^3}$, where $R = \sqrt{r^2 + z^2}$. These Fourier transforms are relatively straightforward to calculate since integrating over ϕ simply gives a 1D Fourier transform in r with the following equation

$$\tilde{f}(q) = 2\pi \int_0^\infty f(x) J_0(qr) dr. \quad (5.4)$$

The Fourier transform of \mathbf{u}^i for a force along the x axis is therefore given by

$$\tilde{\mathbf{u}}_x^i = \frac{F_x}{2G} e^{-q|z|} \left(\frac{q^2 + q_y^2 - qq_x^2}{q^3}, \frac{q_x q_y (1 + q|z|)}{q^3}, -i \frac{q_x |z|}{q} \right). \quad (5.5)$$

The part of \mathbf{u} that depends on ν is given by

$$\mathbf{u}_x^\nu = \frac{F_x (1 - 2\nu)}{4\pi G} \left(\frac{1}{R + |z|}, \frac{x^2}{R(R + |z|)^2}, \frac{xy}{R(R + |z|)^2}, \frac{x}{R(R + |z|)^2} \right). \quad (5.6)$$

However, the Fourier transform can be simplified when it is recognised that this is simply

$$\mathbf{u}_x^v = \left(\frac{\partial}{\partial x}, \frac{\partial}{\partial y}, -\frac{\partial}{\partial |z|} \right) \frac{x}{R+|z|}. \quad (5.7)$$

Therefore to calculate $\tilde{\mathbf{u}}_x^v$ we need to know the Fourier transform of $\frac{x}{R+z}$ and then

use the relation

$$FT \left[\frac{\partial f}{\partial x} \right] = q FT[f], \quad (5.8)$$

where q is the Fourier transform of x . The Fourier transform of $\frac{x}{R+z}$ is given by

$$FT \left[\frac{x}{R+z} \right] = -2\pi i e^{-qz} \frac{q_x}{q^3}. \quad (5.9)$$

Thus, $\tilde{\mathbf{u}}_x^v$ is

$$\tilde{\mathbf{u}}_x^v = 2\pi e^{-q|z|} \frac{q_x}{q^3} (q_x, q_y, -iq). \quad (5.10)$$

Combining the two Fourier transforms gives a Fourier transform for the displacement for a force in the x -direction.

$$\tilde{\mathbf{u}}_x = \frac{F_x}{2G} e^{-q|z|} \left(\frac{2q^2 - (2\nu + q|z|)q_x^2}{q^3}, \frac{q_x q_y (q|z| + 2\nu)}{q^3}, -i \frac{q_x (q|z| + 1 - 2\nu)}{q^2} \right). \quad (5.11)$$

By symmetry the equivalent expression for a force in the y direction is given by

$$\tilde{\mathbf{u}}_y = \frac{F_y}{2G} e^{-q|z|} \left(-\frac{q_x q_y (q|z| + 2\nu)}{q^3}, \frac{2q^2 - (2\nu + q|z|)q_y^2}{q^3}, -i \frac{q_y (q|z| + 1 - 2\nu)}{q^2} \right). \quad (5.12)$$

Therefore combining Eq's (5.11) and (5.12), the Fourier transform of the displacement is given by

$$\tilde{\mathbf{u}}(\mathbf{q}, z) = \frac{\exp(-q|z|)}{2Gq} \left(2\mathbf{F} - (2\nu + q|z|) \frac{\mathbf{q} \cdot \mathbf{F}}{q^2} \mathbf{q}, i(1 - 2\nu + q|z|) \frac{\mathbf{q} \cdot \mathbf{F}}{q} \right), \quad (5.13)$$

where $\mathbf{F} = (F_x, F_y)$ is a force in an arbitrary direction in the plane of the surface and

$\mathbf{q} = (q_x, q_y)$ with $q = \sqrt{q_x^2 + q_y^2}$, $\tilde{\mathbf{u}}$ is a three-dimensional vector with two components in Fourier space $\tilde{u}_{q_x}, \tilde{u}_{q_y}$, and one in real space \tilde{u}_z . This can then be integrated over the

gate. When using the elastic gate model, the only force exerted is round the edge of the gate. There is an element of force $d\mathbf{F} = \bar{F} ds$ for each element of the perimeter, where \bar{F} is the force per unit length and ds is an outward perpendicular. There is also

a phase factor since the force does not originate at the centre of the gate but rather at the edge of the gate a distance r away. Thus

$$\mathbf{F} = \bar{F} \oint \exp(-i\mathbf{q} \cdot \mathbf{r}) ds = -i\mathbf{q}\bar{F} \int \exp(-i\mathbf{q} \cdot \mathbf{r}) dS \equiv -i\mathbf{q}g(\mathbf{q}). \quad (5.14)$$

We define $g(\mathbf{q})$ to be the gate factor, which is determined by the distribution of stress within the gate and so is dependent on both the shape of the gate and the elastic model used to describe the gate. Although this calculation holds for an elastic gate, a similar gate factor can be defined for any distribution of stress in the gate, however it may no longer be proportional to \mathbf{q} . In general, the gate factor is defined to be

$$-i\mathbf{q}g(\mathbf{q}) = \iint \mathbf{F}(\mathbf{r}) \exp(-i\mathbf{q} \cdot \mathbf{r}) dx dy. \quad (5.15)$$

We can thus obtain an expression for the displacement caused by an elastic gate on the surface of an infinite semiconductor, by substituting for the force \mathbf{F} with $-i\mathbf{q}g(\mathbf{q})$ [Eq. (5.14)].

$$\tilde{u}(\mathbf{q}, z) = \frac{g(\mathbf{q}) \exp(-q|z|)}{2Gq} [i(q|z| - 2 + 2\nu)\mathbf{q}, (q|z| + 1 - 2\nu)q] \quad (5.16)$$

The gate factor for a circle of radius a is

$$g^{\circ}(q) = \pi a^2 \bar{F} \frac{2J_1(qa)}{qa}. \quad (5.17)$$

and that for a rectangle that occupies $(\pm a, \pm b)$ is

$$g^{\square}(q) = 4ab\bar{F} \text{sinc}(q_x a) \text{sinc}(q_y b) \quad (5.18)$$

where $\text{sinc } x = \frac{\sin x}{x}$.

5.2 Deformation potential

The deformation potential can also be calculated for island gates. This is simpler because it is proportional to the dilation, which does not depend on the surface or the orientation, within the approximation of an isotropic medium. The dilation from a Cerruti force in the x -direction is

$$\delta(\mathbf{r}) = -\frac{(1-2\nu)F_x x}{2\pi G R^3}. \quad (5.19)$$

The Fourier transform in x and y , when combined with a force along y , is

$$\tilde{\delta}(\mathbf{q}, z) = \frac{i(1-2\nu)}{Gq} \mathbf{F} \cdot \mathbf{q} \exp(-q|z|). \quad (5.20)$$

Once integrated round the gate this becomes

$$\tilde{\delta}(\mathbf{q}, z) = \frac{(1-2\nu)}{G} g(\mathbf{q})q \exp(-q|z|). \quad (5.21)$$

To obtain the potential energy in the 2DEG this is multiplied by Ξ , the deformation potential constant.

$$\tilde{V}_{\text{def}}(\mathbf{q}, z) = \Xi \frac{(1-2\nu)}{G} g(\mathbf{q})q \exp(-q|z|). \quad (5.22)$$

The deformation potential energy is shown in Figure 17. The deformation potential energy can also be calculated directly from Eq. (5.16), recognising that the dilation is the divergence of the displacement. Therefore

$$V_{\text{def}} = \Xi \nabla \cdot \mathbf{u}. \quad (5.23)$$

Whichever method is used for the calculation, the deformation potential can then be screened using the Thomas Fermi dielectric function [Eq. (2.12)] giving

$$\tilde{V}_{\text{def}}(\mathbf{q}, z) = \frac{\Xi}{\epsilon_{TF}(q, \text{depth})} \frac{(1-2\nu)}{G} g(\mathbf{q})q \exp(-q|z|). \quad (5.24)$$

5.3 Piezoelectric potential

The polarisation is given by $P_i = e_{ijk} \epsilon_{jk}$ and the charge density by $\rho = -\nabla \cdot \mathbf{P}$. The strain field is given by

$$\epsilon_{ij} = \frac{1}{2} \left(\frac{\partial u_i}{\partial R_j} + \frac{\partial u_j}{\partial R_i} \right). \quad (5.25)$$

Therefore, the charge density is given by

$$\rho = -\frac{e_{ijk}}{2} \frac{\partial}{\partial R_i} \left(\frac{\partial u_j}{\partial R_k} + \frac{\partial u_k}{\partial R_j} \right) = -e_{ijk} \frac{\partial^2 u_j}{\partial R_i \partial R_k}. \quad (5.26)$$

To find the bare potential ϕ_{bare} , Poisson's equation [Eq. (2.9)] needs to be solved. In real space this is

$$\nabla^2 \phi_{\text{bare}} = -\frac{\rho}{\epsilon_0 \epsilon_r}.$$

To get the potential in the 2DEG the Fourier transform is then screened using Thomas Fermi screening [Eq. (2.12)] to give

$$\tilde{\phi} = \frac{\tilde{\phi}_{\text{bare}}}{\epsilon_{\text{TF}}(q, \text{depth})}. \quad (5.27)$$

No simple approximations for this in real space exist like in the case of the stripe gate, because we do not derive the potential from a harmonic function. Thus, the Fourier transform is required to calculate the potential in the 2DEG. However, some work can be done in real space.

5.4 Piezoelectric potential in real space

Bare potentials for square gates can be calculated, as can charge densities for square and circular gates on all the common surfaces, for the incompressible approximation.

The charge density for the incompressible approximation [Eq. (5.2)] from a single Cerruti force pointing in a direction θ from the [010] axes can be calculated by using the displacement from such a force in the x -direction by Eq. (5.2) in Eq (5.26). When the piezoelectric tensor, e_{ijk} , for [100] is substituted into Eq. (5.26) we get

$$\rho = -2e_{14} \left(\frac{\partial^2 u_x}{\partial y \partial |z|} + \frac{\partial^2 u_y}{\partial x \partial |z|} + \frac{\partial^2 u_z}{\partial x \partial y} \right). \quad (5.28)$$

The resultant charge density for a force in the x -direction [010] is

$$\rho = -\frac{3F_x e_{14} y r}{4\pi G} \frac{14x^2 - y^2 - z^2}{(x^2 + y^2 + z^2)^{7/2}}. \quad (5.29)$$

The charge density for a force in the y -direction can be deduced from this by symmetry

$$\rho = -\frac{3F_y e_{14} x r}{4\pi G} \frac{14y^2 - x^2 - z^2}{(x^2 + y^2 + z^2)^{7/2}}. \quad (5.30)$$

Figure 15 shows this charge density arising from a Cerruti force in the [010],[011],[001] and $[0\bar{1}1]$ directions on the (100) surface. Eq. (5.29) can then be integrated around the edges of the gate in the same manner as the displacement in §5.1 to give the charge density for any shape of gate.

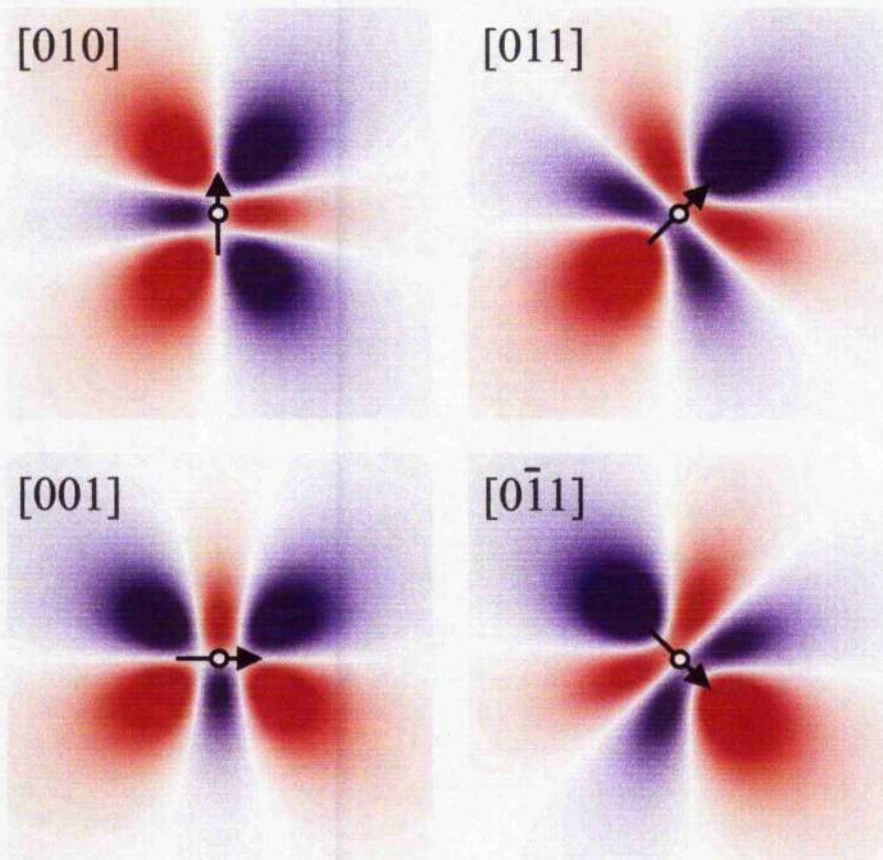


Figure 15 Piezoelectric charge density in a plane 50 nm below a (100) surface due to point forces at the origin, aligned along the [010] crystal axis, the [011] direction, the [001] crystal axis and the [01̄1] direction. Each plot shows an area of $(200 \text{ nm})^2$. Blue is negative charge density, which leads to a positive potential energy and red is positive charge density.

The charge density for a square gate can thus be worked out relatively straight forwardly by integrating round the edges of the gate e.g. for the right side of a square gate, centred on the origin with a width of $2a$, the integral becomes

$$\rho_{RS} = - \int_{-a}^a \frac{3F_x e_{14} (y-Y) r}{4\pi G} \frac{14(x-a)^2 - (y-Y)^2 - z^2}{((x-a)^2 + (y-Y)^2 + z^2)^{7/2}} dY. \quad (5.31)$$

Summing over all four sides results in the following charge density for a square of side $2a$.

$$\rho = \frac{\bar{F}e_{14}r}{4\pi G} \left[\frac{7((x-a)^2 + (y-a)^2) - 2z^2}{((x-a)^2 + (y-a)^2 + z^2)^{5/2}} - \frac{7((x+a)^2 + (y-a)^2) - 2z^2}{((x+a)^2 + (y-a)^2 + z^2)^{5/2}} \right. \\ \left. - \frac{7((x-a)^2 + (y+a)^2) - 2z^2}{((x-a)^2 + (y+a)^2 + z^2)^{5/2}} + \frac{7((x+a)^2 + (y+a)^2) - 2z^2}{((x+a)^2 + (y+a)^2 + z^2)^{5/2}} \right] \quad (5.32)$$

where $\bar{F} = F_x = F_y$ is the magnitude of the force along the edges. As can be seen from Figure 15 a force along the [010] is antisymmetric along the [010] axis, thus a row of such forces, as exists along the edge of a square gate aligned to the crystal axes would cancel except at the ends. Thus for this square gate the charge density cancels out along the sides of the gates, only leaving a charge density under the corners, which is shown by Eq. (5.32). For a gate aligned with the cleavage planes the opposite effect happens, with the charge density cancelling in the corners and only appearing under the edges of the gate. This can be seen in Figure 20.

The bare potential can then be calculated by solving Poisson's equation [Eq. (2.9)]. I have solved this equation by assuming that the potential will take the form

$$\phi_{\text{bare}} = A|z| \left[\frac{B((x-a)^2 + (y-a)^2) + Cz^2}{((x-a)^2 + (y-a)^2 + z^2)^{3/2}} - \frac{B((x+a)^2 + (y-a)^2) + Cz^2}{((x+a)^2 + (y-a)^2 + z^2)^{3/2}} \right. \\ \left. - \frac{B((x-a)^2 + (y+a)^2) + 2z^2}{((x-a)^2 + (y+a)^2 + z^2)^{3/2}} + \frac{B((x+a)^2 + (y+a)^2) + Cz^2}{((x+a)^2 + (y+a)^2 + z^2)^{3/2}} \right] \quad (5.33)$$

I then substituted this into Poisson's equation [Eq. (2.9)] to find the values of the constants A, B and C . Thus the potential produced by a square gate, of side length $2a$, aligned to the crystal axes is given by

$$\phi_{\text{bare}} = -\frac{\bar{F}e_{14}|z|}{32\pi G} \left[\frac{5((x-a)^2 + (y-a)^2) + 2z^2}{((x-a)^2 + (y-a)^2 + z^2)^{3/2}} - \frac{5((x+a)^2 + (y-a)^2) + 2z^2}{((x+a)^2 + (y-a)^2 + z^2)^{3/2}} \right. \\ \left. - \frac{5((x-a)^2 + (y+a)^2) + 2z^2}{((x-a)^2 + (y+a)^2 + z^2)^{3/2}} + \frac{5((x+a)^2 + (y+a)^2) + 2z^2}{((x+a)^2 + (y+a)^2 + z^2)^{3/2}} \right] \quad (5.34)$$

However solving Poisson's equation for general charge densities is extremely difficult and the resultant equations are usually sprawling messes. It is much easier to proceed via the Fourier Transform, which is necessary for screening anyway.

5.5 Piezoelectric potential in Fourier space

Taking Fourier transforms allows the incompressible approximation to be dropped. The Fourier transform of the charge density of a Cerruti force along the x -axis can be calculated by using Eq. (5.28) replacing the derivatives by x and y with multiplication by q_x and q_y [Eq. (5.8)] to give

$$\tilde{\rho} = -2e_{14} \left(q_y \frac{\partial \tilde{u}_x}{\partial |z|} + q_x \frac{\partial \tilde{u}_y}{\partial |z|} + q_x q_y \tilde{u}_z \right). \quad (5.35)$$

This combined with \tilde{u}_x [Eq. (5.11)] for a force in the x -direction gives rise to a charge density

$$\tilde{\rho}_x = -iF_x d_{14} q \exp(-q|z|) \frac{q_y}{q} \left[2 - \frac{q_x^2}{q^2} (3q|z| - 1 + 2\nu) \right]. \quad (5.36)$$

Poisson's equation [Eq. (2.9)] now needs to be solved to find the bare potential. In semi-Fourier space, Poisson's equation is given by

$$\left(q^2 + \frac{\partial^2}{\partial |z|^2} \right) \tilde{\phi}_{\text{bare}} = -\frac{\tilde{\rho}}{\epsilon_0 \epsilon_r}. \quad (5.37)$$

The boundary conditions are the same as the as one-dimensional case Eq. (2.10) or (2.11), modified for three dimensions.

$$\begin{aligned} \phi &\rightarrow 0 \text{ as } x, y, z \rightarrow \infty \\ \phi(x, z=0) &= 0 \end{aligned} \quad (5.38)$$

Solving Poisson's Equation for a force along the x -axis, by assuming the form of the potential and then substituting back into Poisson's equation, reveals the potential to be

$$\tilde{\phi}_{\text{bare}} = -i \frac{d_{14} F_x}{4\epsilon_0 \epsilon_r} |z| \exp(-q|z|) \frac{q_y}{q} \left[4 - \frac{q_x^2}{q^2} (3q|z| + 1 + 4\nu) \right]. \quad (5.39)$$

This when combined with the result for F_y and integrated over the gate, as for the displacement gives

$$\tilde{\phi}_{\text{bare}} = \frac{d_{14}}{8\epsilon_0 \epsilon_r} g(\mathbf{q}) q |z| \exp(-q|z|) [3q|z| - 7 + 4\nu] \sin 2\theta, \quad (5.40)$$

where θ is the azimuthal angle in the xy plane, measured from the [010] axes. With screening the potential energy can be expressed as

$$\tilde{V}(\mathbf{q}, d) = V_0(\mathbf{q}, d)g(\mathbf{q})[3qd - 7 + 4\nu]\sin 2\theta, \quad (5.41)$$

where $-e$ is the electronic charge and V_0 is given by

$$V_0(\mathbf{q}, d) = \frac{-ed_{14}}{8\varepsilon_0\varepsilon_r\varepsilon_{Tz}}qd \exp(-qd). \quad (5.42)$$

5.6 Piezoelectric potential on an arbitrary surface

The piezoelectric potential for a gate on an arbitrary surface is given by

$$\nabla^2 \phi = -\frac{\rho}{\varepsilon_0\varepsilon_r} = \frac{e_{ijk}}{\varepsilon_0\varepsilon_r} \frac{\partial}{\partial R_i} \frac{\partial}{\partial R_j} u_k. \quad (5.43)$$

To simplify calculations it is convenient to define a piezoelectric pseudopotential Φ_i by

$$\nabla^2 \Phi_i = 2Gu_i, \quad (5.44)$$

or in semi-Fourier space

$$\left(q^2 + \frac{\partial^2}{\partial |z|^2} \right) \tilde{\Phi}_i = 2G\tilde{u}_i, \quad (5.45)$$

which holds for all surfaces. Then the potential can be calculated as

$$\phi = \frac{e_{ijk} \partial_i \partial_j \Phi_k}{2G\varepsilon_0\varepsilon_r} = \frac{d_{ijk} \partial_i \partial_j \Phi_k}{\varepsilon_0\varepsilon_r}. \quad (5.46)$$

The boundary conditions can be satisfied by adding any solution of Laplace's equation, thus we only have to solve 3 Poisson's equations for Φ , and we can then calculate the potential on any surface straightforwardly.

To solve this equation for Φ_i , I assumed the form of the potential to be

$$\begin{aligned} \tilde{\Phi}_x &= \frac{|z|e^{-q|z|}}{q^4} (A_1 q^2 + q_x^2 (A_2 + A_3 \nu + A_4 q|z|)), \\ \tilde{\Phi}_y &= \frac{|z|e^{-q|z|}}{q^4} q_x q_y (B_1 + B_2 \nu + B_3 q|z|), \\ \tilde{\Phi}_z &= \frac{|z|e^{-q|z|}}{q^3} i q_x |z| (C_1 + C_2 \nu + C_3 q|z|). \end{aligned} \quad (5.47)$$

Then I substitute this into Eq. (5.45) and determine the constants by comparison with Eq. (5.11). Thus, the piezoelectric pseudopotential for a Cerruti force in the x -direction, F_x , is given by

$$\tilde{\Phi}(\mathbf{q}, z) = -\frac{F_x |z| \exp(-q|z|)}{4q^2} \left(4 - \frac{q_x^2}{q^2} (q|z| + 1 + 4\nu) - \frac{q_x q_y}{q^2} (q|z| + 1 + 4\nu) + i \frac{q_y}{q} (q|z| + 3 - 4\nu) \right). \quad (5.48)$$

The result for a Cerruti force in the y -direction, F_y , is obtained by symmetry.

$$\tilde{\Phi}(\mathbf{q}, z) = -\frac{F_y |z| \exp(-q|z|)}{4q^2} \left(-\frac{q_x q_y}{q^2} (q|z| + 1 + 4\nu) + 4 - \frac{q_y^2}{q^2} (q|z| + 1 + 4\nu) + i \frac{q_x}{q} (q|z| + 3 - 4\nu) \right). \quad (5.49)$$

Combining these results and then integrating round the gate as in §5.1 gives

$$\tilde{\Phi}(\mathbf{q}, z) = -g(\mathbf{q}) \frac{|z| \exp(-q|z|)}{4q^2} [i(q|z| - 3 + 4\nu) \mathbf{q}_x + (q|z| + 3 - 4\nu) \mathbf{q}_y]. \quad (5.50)$$

We can then differentiate this expression, and use the symmetries of the piezoelectric tensor to get the following result for the potential energy

$$\begin{aligned} \frac{\tilde{V}(\mathbf{q}, d)}{V_0(q, d)g(\mathbf{q})} &= \frac{1}{2} (5qd - 9 - 4\nu) \hat{d}_{333} \\ &\quad - \frac{1}{4} i (15qd - 29 - 4\nu) (\hat{d}_{133} \cos \theta - \hat{d}_{233} \sin \theta) \\ &\quad + \frac{1}{2} (3qd - 7 + 4\nu) [(\hat{d}_{223} - \hat{d}_{113}) \cos 2\theta + 2\hat{d}_{123} \sin 2\theta] \\ &\quad + \frac{1}{4} i (qd - 3 + 4\nu) [(\hat{d}_{111} - 3\hat{d}_{122}) \cos 3\theta + (\hat{d}_{222} - 3\hat{d}_{112}) \sin 3\theta] \end{aligned} \quad (5.51)$$

where $\hat{d}_{ijk} = \frac{d_{ijk}}{\frac{1}{2}d_{14}^{(100)}}$.

We can then rotate the piezoelectric tensor e_{ijk} as in §3.4, to obtain the result for the potential on any surface.

Thus the potentials for gates on some common surfaces are

$$\frac{\tilde{V}^{(110)}(\mathbf{q}, d)}{V_0(q, d)g(\mathbf{q})} = -\frac{1}{4} i (15qd - 29 - 4\nu) \cos \theta + \frac{3}{4} i (qd - 3 + 4\nu) \cos 3\theta \quad (5.52)$$

$$\frac{\tilde{V}^{(11)}(\mathbf{q}, d)}{V_0(q, d)g(\mathbf{q})} = -\sqrt{\frac{1}{3}}(5qd - 9 - 4\nu) + i\sqrt{\frac{2}{3}}(qd - 3 + 4\nu)\sin 3\theta \quad (5.53)$$

$$\begin{aligned} \frac{\tilde{V}^{(311)}(\mathbf{q}, d)}{V_0(q, d)g(\mathbf{q})} &= -\frac{9}{11}\sqrt{\frac{1}{11}}(5qd - 9 - 4\nu) - \frac{24}{11}\sqrt{\frac{1}{11}}(3qd - 7 + 4\nu)\cos 2\theta \\ &\quad - i\frac{4}{11}\sqrt{\frac{2}{11}}(15qd - 29 - 4\nu)\sin \theta \\ &\quad + i\frac{15}{11}\sqrt{\frac{2}{11}}(qd - 3 + 4\nu)\sin 3\theta \end{aligned} \quad (5.54)$$

The one-dimensional results can be deduced from this result, and shown to be consistent with §3.3-3.4. If we take the width of the gate to lie along the y -axis and the current (either for a FET or in a LSSL magnetoresistance experiment) to pass along the x -axis, then we can calculate a new gate factor $g^{\parallel}(\mathbf{q})$, by taking the limit as the width tends to infinity for a rectangular gate (5.18).

$$\lim_{b \rightarrow \infty} g^{\square}(q) = 2\pi\delta(q_y) \times 2a\bar{F} \operatorname{sinc} q_x a \equiv 2\pi\delta(q_y)g^{\parallel}(q_x) \quad (5.55)$$

The inverse Fourier transform of $2\pi\delta(q_y)$ simply gives unity showing that the potential does not depend on y as expected. Thus we can find the results for a stripe gate by choosing q_x as the direction of the current by rotating \mathbf{q} by θ° from the principal axis in the plane of the surface and then setting $q_y = 0$, and $g(\mathbf{q}) = g^{\parallel}(q_x)$.

5.7 Results

The results of the screened potentials energies in a 2DEG 50 nm below circular Ti gates of diameter 100 nm and 30nm thick which are strained by +0.001, on various surfaces are shown in Figure 16. It can clearly be seen that the $\bar{4}3m$ symmetry of the semiconductor breaks the circular symmetry of the gate. On the (100) surface, the potential is proportional to $\sin 2\theta$. It reaches a maximum of around ± 0.4 meV. The potential crosses 0 twice as r is increased for the dimensions plotted in Figure 16 but this varies with depth. As can be seen from Figure 17 the potential does not just decay with increasing depth but rather changes shape and sign with varying depth. The effect of including a parasitic channel of electrons trapped around the donor layer is also shown. In this case the effect of screening is not large, with the potential growing slightly larger. The deformation potential is also shown, which can be seen to be

much smaller than the piezoelectric potential for these parameters. The deformation potential also has circular symmetry and so unlike the piezoelectric potential reflects the symmetry of the gate.

The (110) surface is antisymmetric along the $[\bar{1}\bar{1}0]$ axis, and symmetric along the [001] axis. The magnitude of the potential is also larger than on the (100) surface. The (111) surface is very interesting because it almost preserves the symmetry of the gate due to the $\sin 3\theta$ term being much weaker than the dominant isotropic term, by a factor of around 1/3. Thus for the circular gate shown the potential has roughly circular symmetry. The magnitude is much larger than (100), around -1 meV, for these parameters. The (311) surface has more terms, which lower the overall symmetry, leaving only one symmetry plane, $[\bar{2}33]$. The potential is smaller than (111) but larger than the (100) surface. Square gates can also be calculated; plots of arrays of square gates for the (100) surface are shown in Figure 20.

The piezoelectric potential is larger than the deformation potential for electrons in the devices considered here; however holes are more complicated and the deformation potential may impact them more. The ratio between the two potentials is given by

$$\frac{\tilde{V}_{\text{piezo}}(q)}{\tilde{V}_{\text{def}}(q)} = \frac{ee_{14}}{8\epsilon_0\epsilon_r(1-2\nu)\Xi} d[3qd - 7 + 4\nu], \quad (5.56)$$

which depends on the size of the gate. The deformation potential becomes more important as the size of the gate shrinks³⁹. This works out at around 5 for the surfaces and gates considered here.

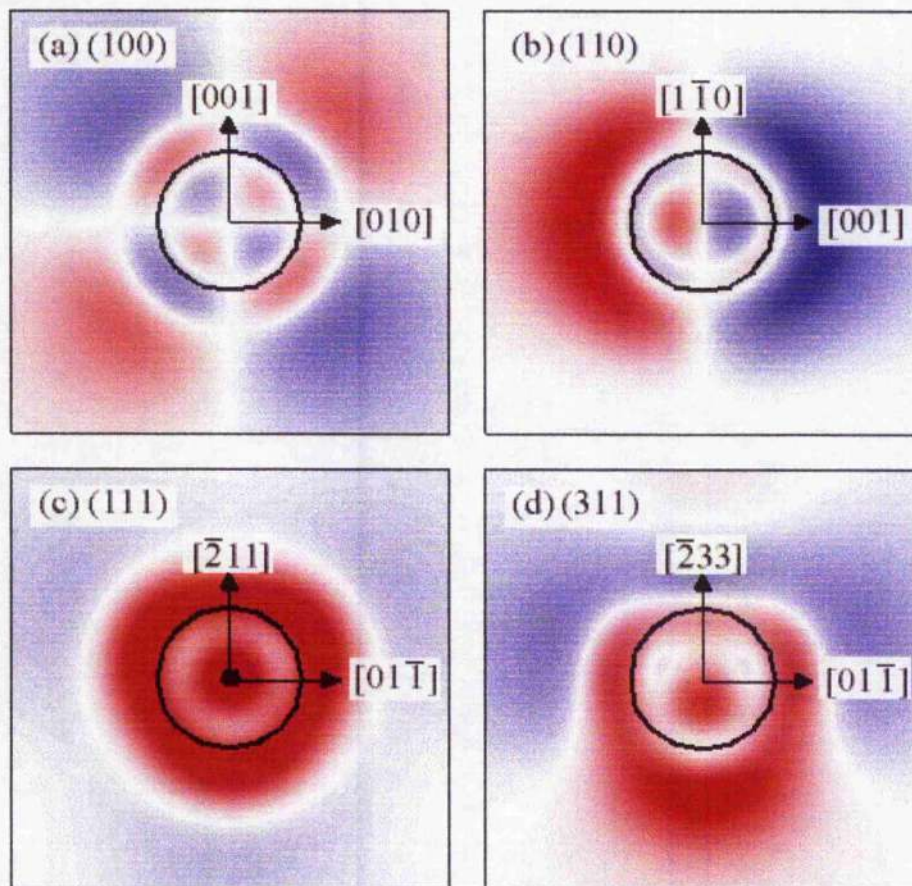


Figure 16 Screened piezoelectric potential energy in a 2DEG situated 50 nm below circular gates of diameter 100 nm (black outline) on different surfaces. The scale goes from -1.5 meV (blue) through 0 meV (white) to $+1.5$ meV (red).

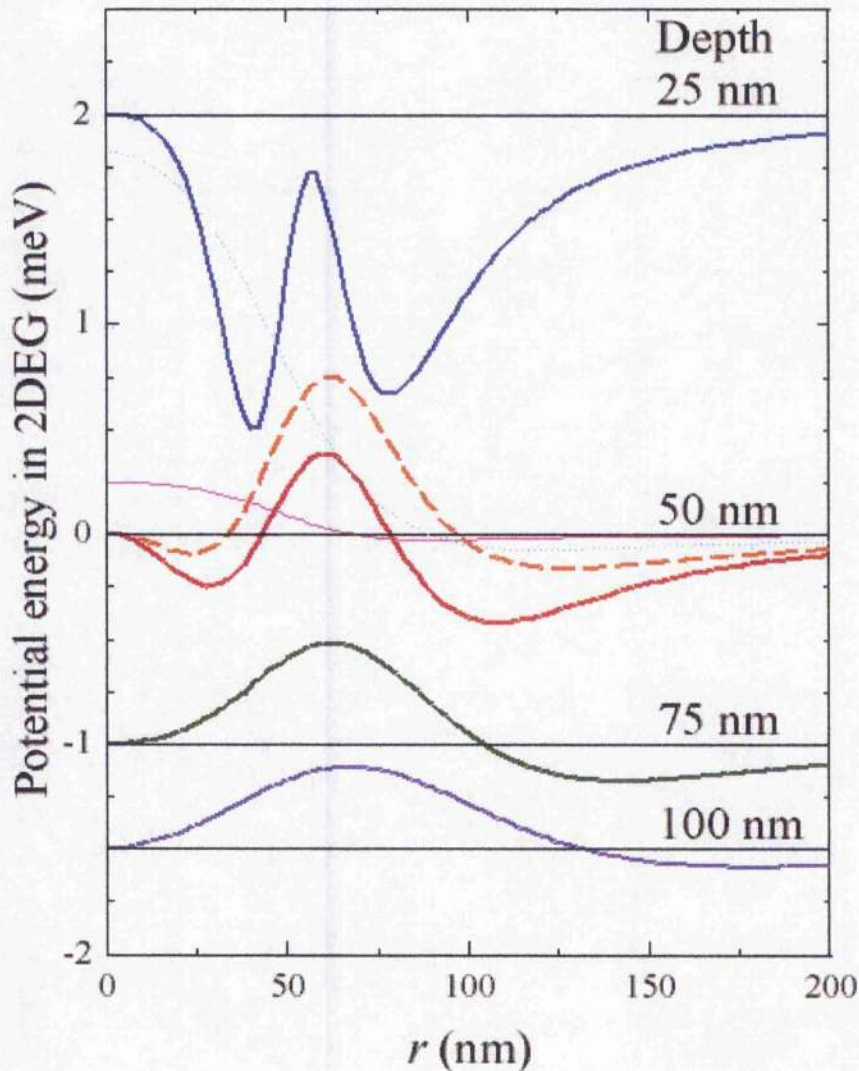


Figure 17 Screened piezoelectric potential energy in 2DEG's of different depths under a circular gate of diameter 100 nm on a (100) surface (thick lines). The radius is along [011], where the piezoelectric effect reaches its maximum. Curves are offset for clarity as shown by horizontal lines. The effect of additional screening by a parasitic layer of electrons around the donors, 25 nm deep, is shown for the 50-nm depth (broken thick orange line). The screened deformation potential energy (thin purple line) has circular symmetry, and the corresponding bare energy (thin dotted cyan line) is proportional to the dilation; both are for a depth of 50 nm with no parasitic layer.

5.8 Conclusions

I have shown how to calculate the deformation potential and piezoelectric potential for an arbitrary gate shape on an arbitrary surface. I have calculated the deformation potential for rectangular, square and circular gates and the piezoelectric potential for rectangular, square and circular gates on the (100), (110), (111) and (311) surfaces.

Unlike the stripe gates, it is not possible through choice of surface, orientation or dimensions to build square or circular gates, which do not produce a piezoelectric potential. However, it is possible to vary these parameters to design a gate to minimise these effects or to produce a potential with a variety of symmetries.

The piezoelectric potentials generated do not in general have the same symmetry as the gates that produce them. However, the (111) surface produces a potential with almost the same symmetry as the gate, due to the dominant isotropic term. This makes (111) attractive for experiments where the potential is required to be the same along both axes. (111) is also attractive for experiments that are designed to harness the piezoelectric potential because it has the largest potential of all the surfaces, around 1 meV for the dimensions used here.

Square gates aligned to the crystal axes on (100) surface, produce potentials that are concentrated under the corners of the gates, while square gates aligned to the cleavage planes produce a potential under their sides and not the corners.

Electrons and holes can be confined by these gates, if the potentials are made large enough, either by increasing the size of the gate or the strain. However, due to the symmetries and variation with the radius of piezoelectric potentials, the confinement of electrons and/or holes underneath gates is non-trivial. Gates on the (100) surface have the effect that they trap electrons and holes in separate places. Gates on (111) will confine electrons under the centre of the gate if they are produced by a strained layer, such as InGaAs, or in a ring between the centre of the gate and the edge if it is a metal gate. A gate on (110) will trap electrons under one side of the gate but not the other.

The deformation potential does reflect the symmetry of the gate. However due to its much smaller size it can usually be neglected when considering electrons in AlGaAs. This will no longer be the case if holes are being considered or other semiconductors are being used which have a smaller piezoelectric constant.

A bias can also be applied to a metal gate, which produces a potential that has the symmetry of the gate. When added to the built in piezoelectric potential this breaks the symmetry even further, resulting in areas of large negative potential and small positive potential, or vice versa depending on the sign of the applied bias.

6 Two-dimensional Lateral Surface Superlattices

6.1 Extension to Lateral Surface Superlattices

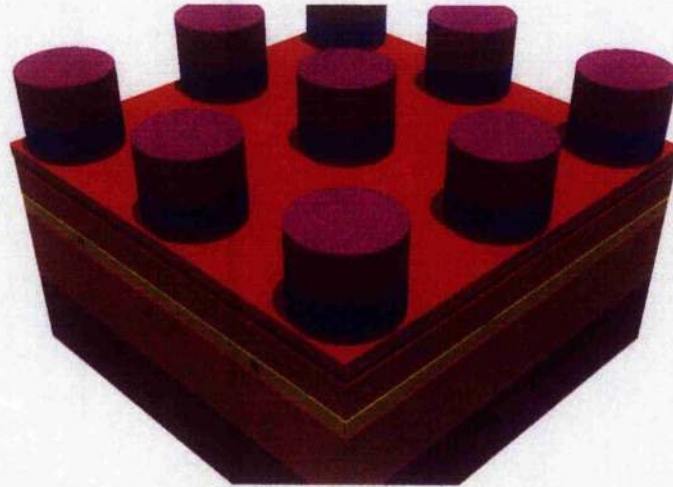


Figure 18 A section of a two-dimensional LSSL, with circular gates, made by etching InGaAs layers. Purple - GaAs, Red - AlGaAs, Yellow - Delta doped AlGaAs, Blue - InGaAs.

It is straightforward to extend the results for the Fourier transform of the potential produced by a single gate to that for an array of gates (a 2D LSSL), as shown in Figure 18. For a square array of gates aligned along the principal axes x and y , with period b , the Fourier transform of the potential for a single gate must be changed to a Fourier series. This is achieved by limiting the coefficients to the wave vectors of the reciprocal lattice and dividing the Fourier Transform by b^2 .

$$V(x, y) = \frac{1}{b^2} \sum_{m, n} \tilde{V}(q_{mn}) \exp(iq_m x) \exp(iq_n y) \quad (6.1)$$

The reciprocal lattice vectors are given by

$$q_{mn} = \frac{2\pi}{b} (m, n). \quad (6.2)$$

Thus the Fourier coefficients for a square array of gates aligned to the crystal axes on a (100) surface can be written as

$$\tilde{V}_{mn}(d) = \frac{V_0(q,d)g(q_{mn})}{b^2} [3q(d+c) - 7 + 4\nu] \frac{2mn}{m^2 + n^2}, \quad (6.3)$$

where $q = (2\pi/b)\sqrt{m^2 + n^2}$, when the $\sin 2\theta$ term is written in terms of q . This potential is shown in Figure 20. The symmetry of the piezoelectric effect causes this to vanish for $m=0$ or $n=0$, which includes the fundamental components $((m,n) = (\pm 1, 0)$ and $(m,n) = (0, \pm 1)$). The smallest surviving Fourier components have $(m,n) = (\pm 1, \pm 1)$. These can be combined into two cosines that vary along directions at $\pm 45^\circ$ to the principal axes of the crystal and the array. Each has a peak value of 0.11 meV for circular gates with $a=100$ nm in an array with $b=200$ nm. Adding the two cosines gives a spacial dependence of

$$V(x,y,d) \approx -4 \frac{V_0(q',d)g(q')}{b^2} [3q'd - 7 + 4\nu] \sin \frac{2\pi x}{b} \sin \frac{2\pi y}{b}, \quad (6.4)$$

where $q' = 2\sqrt{2}\pi/b$. The linear period of this potential is smaller than that of the gates by a factor of $\sqrt{2}$.

The Fourier coefficients for a square array aligned to the cleavage planes can be found by rotating this through 45° , giving a factor of $\cos 2\theta$ instead of $\sin 2\theta$.

$$\tilde{V}_{nm}(d) = \frac{V_0(q,d)g(q_{nm})}{b^2} [3q(d+c) - 7 + 4\nu] \frac{m^2 - n^2}{m^2 + n^2} \quad (6.5)$$

This potential is also shown in Figure 20. The fundamental components now survive, and give

$$V(x',y',d) \approx 2 \frac{V_0(q'',d)g(q'')}{b^2} [3q''d - 7 + 4\nu] \left(\cos \frac{2\pi x'}{b} - \cos \frac{2\pi y'}{b} \right), \quad (6.6)$$

where $q'' = 2\pi/b$. This has a peak value in each direction of 0.19 meV for our example of a 2DEG at a depth of 50nm beneath an array with period 200nm, of Ti gates of width 100nm and height 30nm, strained by +0.001.

It is also relatively straightforward to extend these results to an array of gates, where the gates are set in a square array but they touch at the corners, as shown in Figure 19. We have chosen to call this configuration the "chess board". This is achieved through a structure function that defines the unit cell. This is given by

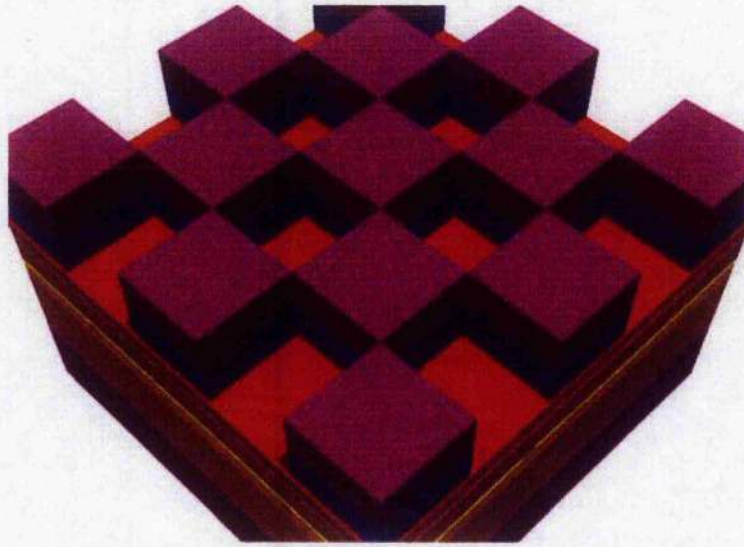


Figure 19 A section of a two-dimensional LSSL, in chessboard layout i.e. square gates touching at the corners, made by etching InGaAs layers. Purple - GaAs, Red - AlGaAs, Yellow - Delta doped AlGaAs, Blue - InGaAs.

$$\begin{aligned}
 sf &= 1 + \exp\left(i\mathbf{q} \cdot \left(\frac{a}{2}, \frac{a}{2}\right)\right) \\
 &= 1 + e^{i\pi(m+n)} \\
 &= \begin{cases} 2 & (m+n) \text{ even} \\ 0 & (m+n) \text{ odd} \end{cases}
 \end{aligned} \tag{6.7}$$

Therefore, the potential from a chessboard array of gates aligned to the crystal axes is given by

$$\tilde{V}_{mn}(d) = \frac{V_0(q, d)g^{\square}(q_{mn})}{b^2} [3q(d+c) - 7 + 4v] [1 + e^{i\pi(m+n)}] \frac{2mn}{m^2 + n^2}. \tag{6.8}$$

This can be seen in Figure 21. At first glance this looks the same as for a normal array of gates. However, the magnitude is greater, since the potentials arising from the corners of touching gates add.

The potential from the array aligned to the cleavage planes is given by

$$\tilde{V}_{mn}(d) = \frac{V_0(q, d)g^{\square}(q_{mn})}{b^2} [3q(d+c) - 7 + 4v] [1 + e^{i\pi(m+n)}] \frac{m^2 - n^2}{m^2 + n^2}. \tag{6.9}$$

This can also be seen in Figure 21. The potential is much more symmetric with the potential in the areas without gates becoming the inverse of the areas with gates. This is to be expected since the chessboard can be equivalently defined as either an array of

dots or anti-dots and our model assumes that the only difference between the potential produced by dots and anti-dots is the sign of the effect.

The potentials for gates on the surfaces considered can be deduced from Eqs. (5.52), (5.53) and (5.54) and are given by

$$\begin{aligned} \frac{\tilde{V}_{mn}^{(110)}(d)}{V_0(q,d)g(q_{mn})} = & -\frac{1}{4}i(15qd - 29 - 4\nu)\frac{m}{\sqrt{m^2 + n^2}} \\ & + \frac{3}{4}i(qd - 3 + 4\nu)\frac{m^3 - 3mn^2}{(m^2 + n^2)^{3/2}} \end{aligned} \quad (6.10)$$

$$\frac{\tilde{V}_{mn}^{(111)}(d)}{V_0(q,d)g(q_{mn})} = -\sqrt{\frac{1}{3}}(5qd - 9 - 4\nu) + i\sqrt{\frac{2}{3}}(qd - 3 + 4\nu)\frac{3m^2n - n^3}{(m^2 + n^2)^{3/2}} \quad (6.11)$$

$$\begin{aligned} \frac{\tilde{V}_{mn}^{(311)}(d)}{V_0(q,d)g(q_{mn})} = & -\frac{9}{11}\sqrt{\frac{1}{11}}(5qd - 9 - 4\nu) - \frac{24}{11}\sqrt{\frac{1}{11}}(3qd - 7 + 4\nu)\frac{m^2 - n^2}{m^2 + n^2} \\ & - i\frac{4}{11}\sqrt{\frac{2}{11}}(15qd - 29 - 4\nu)\frac{n}{\sqrt{m^2 + n^2}} \\ & + i\frac{15}{11}\sqrt{\frac{2}{11}}(qd - 3 + 4\nu)\frac{3m^2n - n^3}{(m^2 + n^2)^{3/2}} \end{aligned} \quad (6.12)$$

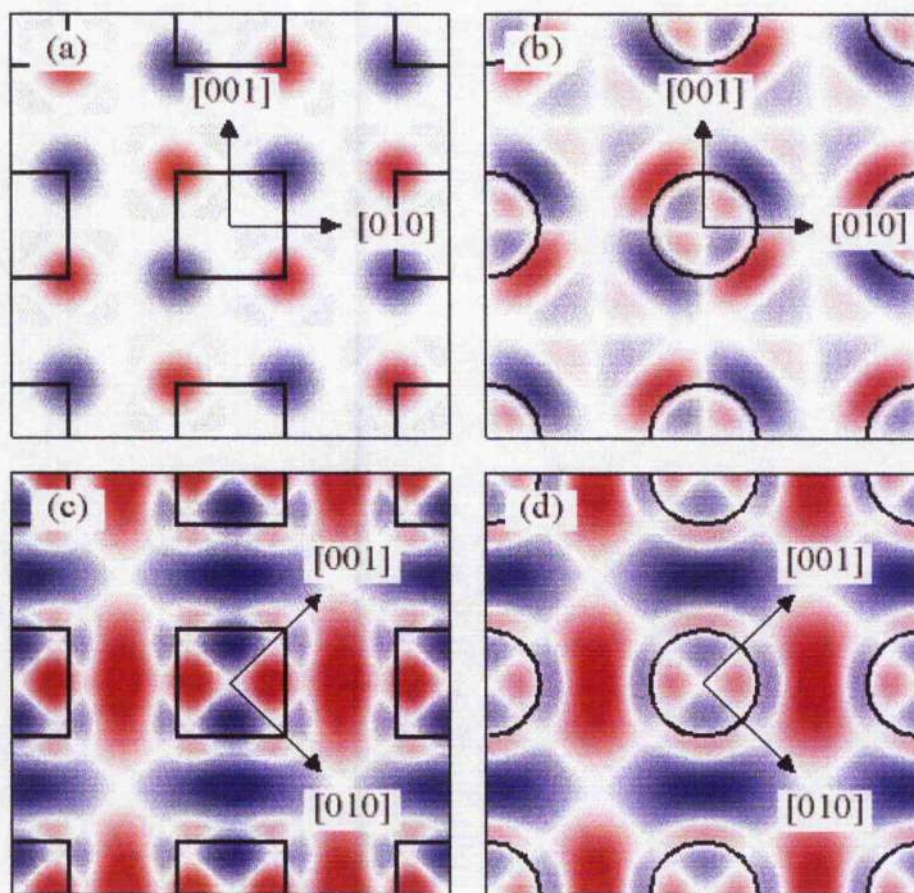


Figure 20 Screened piezoelectric potential in a 2DEG of depth 50 nm below arrays of Ti gates on a (100) surface. They are aligned to the crystal axes in (a) and (b) and to the cleavage planes in (c) and (d). The gates (black outline) have width or diameter of 100 nm, a height of 30nm and are strained by +0.001. The arrays are square and have a period of 200 nm. The scale goes from -1 meV (blue) through 0 meV (white) to +1 meV (red).

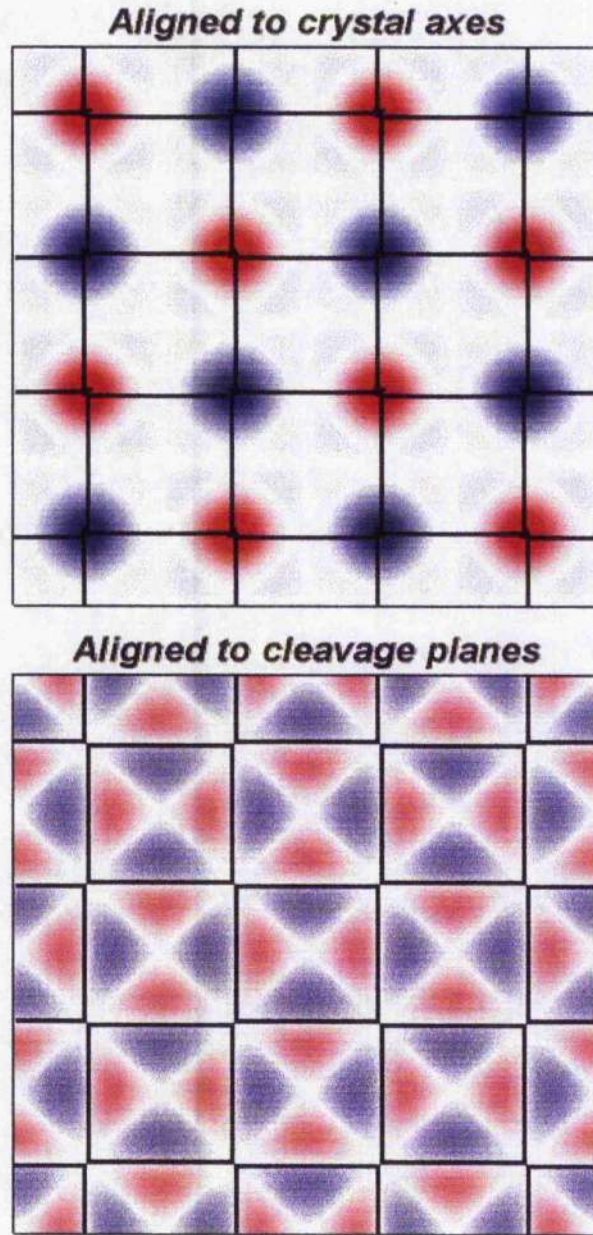


Figure 21 Screened piezoelectric potential in a 2DEG of depth 50 nm below array of Ti gates on a (100) surface. The gates (black outline) have width or diameter of 100 nm, a height of 30nm and are strained by +0.001. They are arranged in a square chess board array of period 200 nm and the scale goes from -1 meV (blue) through 0 meV (white) to +1 meV (red).

6.2 Conclusions

I have shown how to calculate the piezoelectric and deformation potentials arising from a 2D LSSL of arbitrary orientation, on an arbitrary surface, composed of gates of an arbitrary shape. I have calculated the piezoelectric potentials arising from a 2D LSSL composed of square and circular gates on the (110), (111) and (311) surfaces aligned to the crystal axes. On (100) I have calculated the piezoelectric potentials arising from 2D LSSLs aligned with the crystal axes and the cleavage planes of both square and circular gates. I have also calculated the potentials arising from a chessboard configuration of square gates on (100).

While the potentials arising from arrays and gates aligned to the crystal axes are invariant for current travelling in the x or y directions, this is not true when the arrays and gates are aligned along the cleavage planes. If the current flows along $[011]$ then it faces an array of barriers with breaks in the direction perpendicular to current flow where there are channels for the electrons to flow down. However, if the current flows along $[0\bar{1}1]$ then it faces an array of troughs with breaks in the directions perpendicular to current flow where there are barriers to the electron flow. This should lead to different transport properties for the two directions, and could provide a possible route for manufacturing arrays with broken symmetry⁴¹.

Although experiments on 2D LSSLs are not extensive, the drive to understand the commensurability oscillations for a 2D LSSL and the search for Hofstadter butterfly¹⁶ like structures means that more experiments are planned. The calculation of these potentials should prove useful in these experiments and in simulations of 2D LSSLs.

Although it is not possible to work out a simple period halving like in the 1D case, due to the more complex geometry, it is possible to null certain Fourier components and maximise or minimise the potential. For example, on (100) if the array is aligned along the cleavage planes rather than the crystal planes, then even for identical gates with identical spacing the potential is larger. This effect is compounded if square gates are used and the edges of the gates are chosen to align with the array. However, this is not true if the chessboard array is used. While it is true that the potentials are

7 Conclusions

I have calculated the deformation and piezoelectric potential energy under single gates of arbitrary shape and one- and two-dimensional lateral surface superlattices on an arbitrary surface of a cubic III-V semiconductor. These potentials are generated by strain, either due to differential thermal contraction of the gates with respect to the semiconductor, or by a deliberately strained layer grown into the heterostructure. The deformation potential is independent of orientation, within the isotropic approximation for the elastic behaviour, but the piezoelectric potential varies strongly with orientation. These calculations show that the piezoelectric potentials cannot be ignored in III-V semiconductor devices. Furthermore, it is possible to use my calculations to harness the piezoelectric effect to provide the modulation of electrons in devices.

One example where this has been used effectively is in LSSL experiments at Glasgow in which a 2DEG is patterned with an etched stressor layer⁴. These layers have produced potentials with magnitudes of several meV. It has been possible to cancel the fundamental component of the piezoelectric potential leaving only the second harmonic, effectively halving the period of the potential. This technique has promise for creating very short period LSSL with the goal of observing Bloch oscillations and other quantum effects.

Unfortunately, my calculations also show that a similar halving of the period is not possible for island gates. However, it is possible to decrease the period of an array of square gates by a factor of $\sqrt{2}$ if they are aligned to the crystal axes instead of the cleavage planes, to which gates are normally aligned, and the current flows at 45° to the array. It is also possible to produce different effects according to the symmetry of the surface. While (111) has a dominant isotropic term, other surfaces produce totally potentials with totally different symmetries in perpendicular directions, for example when an array of gates is aligned along the cleavage planes of (100). If the current flows along [011] then it faces an array of barriers with breaks in the direction perpendicular to current flow where there are channels for the electrons to flow down. However, if the current flows along $[0\bar{1}1]$ then it faces an array of troughs with

breaks in the directions perpendicular to current flow where there are barriers to the electron flow. This should lead to different transport properties for the two directions. Experiments and simulations of magnetoresistance in two-dimensional LSSIs have been conducted at Glasgow using my calculations to design the experiment and to help interpret the results and more are planned. However, at the moment they are not well understood and more research is necessary.

However, when the devices considered are FETs then the goal is usually to minimise any piezoelectric effects. If the FET can be modelled by a simple stripe gate then on the (100) surface the piezoelectric effect can be eliminated by aligning the gate to the crystal axes. Unfortunately, this is not possible on other surfaces, although my calculations can be used to minimise the effect, and the deformation potential is always present although it is generally much smaller than the piezoelectric effect. The piezoelectric potential is typically around 1 meV for a metal gate on (100).

The island gates are also of interest to quantum dot experiments. The piezoelectric potentials do not reflect the symmetry of the gate and therefore have important implications for the confinement of electrons and holes under such gates. Without the application of an electrostatic potential the electrons and holes will be confined in different areas under the gates, and usually not under the centre of the gate. The deformation potential does reflect the symmetry of the gate, however due to its much smaller size it can usually be neglected when considering electrons in AlGaAs. However, this will no longer be the case if holes are being considered or other semiconductors are being used which have a smaller piezoelectric constant. The deformation potential also becomes more prominent as the size of the dots is reduced.

Thus, I have shown that strain cannot be ignored when either designing or modelling devices on III-V semiconductors. I have also calculated the main potentials arising from gates of arbitrary shape on arbitrary surfaces, which should prove to be useful when designing or modelling these structures.

Future work is needed to better account for some of the assumptions and approximations that I have made. It should be relatively straightforward to account for bending in the gates and the forces perpendicular to the surface that arise from this.

Preliminary work on this has been done³¹. It should also be possible to have a better elastic model for the interaction of the gate and the substrate, particularly in the case of the stressor layer where the interaction is well understood. However, how far these approximations can be relaxed and an analytic solution retained is unknown. I have also only looked briefly at the effects of the piezoelectric effect on FET characteristics. This is another area that could be explored more fully in further research.

8 Bibliography

- 1 S. Adachi, *J. Appl. Phys.* **58**, R1 (1985)
- 2 R. Cuscó, M. R. Holland, J. H. Davies, I. A. Larkin, E. Skuras, A. R. Long, and S. P. Beaumont, *Surf. Sci.* **305**, 643 (1994)
- 3 J. H. Davies and I. A. Larkin, *Phys. Rev. B* **49**, 4800 (1994).
- 4 C. J. Emeleus, B. Milton, A. R. Long, J. H. Davies, D. E. Petticrew, and M. C. Holland, *Appl. Phys. Lett.* **73**, 1412 (1998)
- 5 L. D. Landau, E. M. Lifshitz, A. M. Kosevich, and L. P. Pitaevskii, *Theory of Elasticity* (Pergamon, Oxford, 1986).
- 6 J. F. Nye, *Physical properties of Crystals* (Oxford University Press, Oxford, 1957)
- 7 C. J. Emeleus, B. Milton, A. R. Long, J. H. Davies, D. E. Petticrew, and M. C. Holland, *Superlattices and Microstructures* **25**, 29 (1999)
- 8 I. A. Larkin, J. H. Davies, A. R. Long, and R. Cuscó, *Phys. Rev. B* **56**, 15242 (1997).
- 9 J. C. Ramirez, P. J. McNally, L. S. Cooper, J. J. Rosenberg, L. B. Freund, and T. N. Jackson, *IEEE Trans. Electron Devices* **35**, 1232 (1988)
- 10 J. H. Davies, D. E. Petticrew, and A. R. Long, *Phys. Rev. B* **58**, 10789 (1998).
- 11 D. E. Petticrew, J. H. Davies, A. R. Long, I. A. Larkin, *Physica B* **249-251**, 900 (1998)
- 12 J. H. Davies, *The Physics of Low Dimensional Semiconductors: An Introduction* (Cambridge University Press, Cambridge, 1998)
- 13 A. R. Long, J. H. Davies, M. Kinsier, S. Vallis, and M. C. Holland, *Semicond. Sci. Technol.* **8** 1581-1589 (1993)
- 14 A. R. Long, E. Skuras, S. Vallis, K. Ali, R. Cuscó, I. A. Larkin, J. H. Davies, and M. C. Holland (unpublished)
- 15 E. Skuras M. C. Holland, C. J. Barton, J. H. Davies, A. R. Long, *Semicond. Sci. Technol.* **10**, 922 (1995)
- 16 D. R. Hofstader, *Phys. Rev. B* **14**, 2239 (1976)
- 17 D. Weiss, K. von Klitzing, K. Ploog, and G. Weimann, *Europhys. Lett.* **8**, 179 (1989)
- 18 J. P. Lu, and M. Shayegan, *Phys. Rev. B* **58**, 1138 (1998)
- 19 R. R. Gerhardts, D. Weiss, and K. von Klitzing, *Phys. Rev. Lett.* **62**, 1173 (1989)

- 20 R. W. Winkler, J. P. Kotthaus, and K. Ploog, Phys. Rev. Lett. **62**, 1177 (1989)
- 21 G. Müller, P. Streda, D. Weiss, K. von Klitzing, and G. Weimann, Phys. Rev. B **50**, 8938 (1994)
- 22 C. J. Beenakker, Phys. Rev. Lett. **62**, 2020 (1989)
- 23 P. H. Beton, E. S. Alves, P. C. Main, L. Eaves, M. W. Dellow, M. Henini, O. H. Hughes, S. P. Beaumont and C. D. W. Wilkinson, Phys. Rev. B **42**, 9229 (1990)
- 24 P. H. Beton, M. W. Dellow, P. C. Main, E. S. Alves, L. Eaves, S. P. Beaumont, and C. D. W. Wilkinson, Phys. Rev. B **4**, 9980 (1991)
- 25 R. R. Gerhardts, Phys. Rev. B **45**, 3449 (1992)
- 26 A. D. Mirlin, and P. Wolfe, Phys. Rev. B **58**, 12986 (1998)
- 27 Zhang, and Gerhardts, Phys. Rev. B **41**, 12850 (1990)
- 28 Y. Paltiel, U. Meirav, D. Mahalu, and H. Strikman, Phys. Rev. B **56**, 6416 (1997)
- 29 P. Bøggild, A. Boiser, K. Birkeland, C. B. Sørensen, R. Taborski, and P. E. Lindelof, Phys. Rev. B **51**, 7333 (1995)
- 30 R. R. Gerhardts, Phys. Rev. B **53** 11064 (1996)
- 31 J. H. Davies private communication
- 32 D. Pfannkucke, and R. R. Gerhardts, Phys. Rev. B **46** 12600 (1992)
- 33 P. M. Asbeck, C.-P. Lee, and M.-C. F. Chang, IEEE Trans. Electron Devices **31**, 1377 (1984).
- 34 H. M. Westergaard, *Theory of Elasticity and Plasticity* (Harvard University Press, Cambridge, MA, 1952)
- 35 F. Stern and S. Das Sarma, Phys. Rev. B **30**, 840 (1984)
- 36 J. B. Yau, J. P. Lu, H. C. Manoharan, and M. Shayegan, paper presented at Otta EP2DS to be published in Physica D
- 37 R. Cuscó, E. Skuras, S. Vallis, M. C. Holland, A. R. Long, S. P. Beaumont, I. A. Larkin, and J. H. Davies, Superlattices Microstruct. **16**, 283 (1994)
- 38 R. J. Luyken, A. Lorke, A. M. Song, M. Gossard, Appl. Phys. Lett. **73**, 1110 (1998)
- 39 M. Grundmann, O. Stier, and D. Bimberg, Phys. Rev. B **52**, 11969 (1995)
- 40 C. Albercht, J. H. Smet, D. Weiss, K. von Klitzing, V. Umansky, and H. Schweizer, Physica B **249-251**, 914 (1998)
- 41 A. Lorke, S. Wimmer, B. Jager, J. P. Kotthaus, W. Wegscheider, and M. Bichler, Physica B **249-251**, 312 (1988)